SRL INTERNAL REPORT #75

ELEMENT AND ISOTOPE IDENTIFICATION FROM HIST DATA SUBSEQUENT TO THE DECEMBER 1, 1978 READOUT FAILURE

H. Breneman
December 10, 1980

I. INTRODUCTION

The design and normal operational mode of the Heavy Isotope Spectrometer Telescope (HIST) on board ISEE-3 are described in Refs. 1 and 2; the reader is assumed to be familiar with these. A readout logic failure on December 1, 1978, 109 days into the mission, resulted in the loss of half of the bits of data associated with each event subsequently observed. This report will describe how the degraded data can be used to obtain information on the relative abundances of elements, and of isotopes of a given element, in various energy intervals.

The original event data format for HIST is shown in Fig. 1; the bits lost due to the failure are indicated. The consequences of the failure which are relevant to this discussion are the following:

(1) Loss of the 1st, 2nd, 5th, 6th, 9th and 10th most significant bits of the 12-bit pulse height channel numbers, i.e. those bits corresponding to 2048, 1024, 128, 64, 8 and 4 channels.

(2) Loss of the two most significant bits from the 4-bit range number. This results in ambiguity between ranges 0, 4 and 8, between 1, 5 and 9, between 2 and 6, and between 3 and 7. But in most cases ranges 0 and 1 can still be uniquely identified, by the fact that fewer pulse heights are returned for these events.

(3) Loss of certain bits from the matrix detector addresses, resulting in trajectory and angle ambiguities.

(4) Neither the low-Z ($Z < 3$) bit nor the MH (multiple hodo) bit was affected by the failure.

Subsequent actions taken to optimize data return were:

(1) Deactivation of detectors D6, D7, and D8, to remove the remaining range ambiguities. Thus only ranges 0 through 4 are usable. (Range 5 data is returned, but mixed with range 6, 7, and 8 data.)

(2) Deactivation of the outer 4 strips on each side of the matrix detectors, to form a 16 x 16 array. This was a compromise between reducing trajectory ambiguity and retaining as large a geometry factor as possible (about one-third of the original).

Since the low-Z bit was not lost, the problem of separating low-Z species (mainly protons and alpha particles) could be considered independently of all other species. The object was to determine, for each range from 0 to 4, over what energy intervals protons and alphas could be separated using the bits of pulse height data available. This report will describe the methods and algorithms used to extract this information; give examples of these methods applied to different situations using actual flight data; point out some instrument problems and anomalies uncovered in the course of this work; and describe how the methods developed here can be applied to the tasks of separating the high-Z elements and separating the isotopes of a given element.

II. METHOD

The pulse height channel numbers for low-Z species are never greater than about 110, so the 256- and 512-bits, although still returned by the instrument, are not useful here. Also, the fluctuations in pulse heights due to angle variation, detector thickness variation, Landau fluctuations, etc., are on the order of a few channels, so the 1- and 2-bits are also of no use. This leaves only the 16- and 32-bits. For a given event, one can assign, for each pulse height returned, an integer from 1 to 4 depending on the values of the 16- and 32-bits.

1 if 16-bit and 32-bit both off
2 if 16-bit on and 32-bit off
3 if 16-bit off and 32-bit on
4 if 16-bit and 32-bit both on

Thus each event in range 0 has associated with it a 2-digit combination (16 total possible); each range 1 event, a 3-digit combination (64 possible); each range 2 event, a 4-digit combination (256 possible); and each range 3 or 4 event, a 5-digit combination (1024 possible). By convention, the numbers in the n-digit combination are listed starting from the innermost (or stopping) detector (PHA1) outward.

A FORTH program was written that would calculate the n-digit combination (hereafter referred to as a "bin") for each event, and count the number of events, meeting selected range, time and coincidence requirements, that fall into selected bins. Using data obtained prior to the instrument failure, it was possible to determine the bins occupied by "known" protons and alpha particles (as defined by a "box" drawn around the track on a crossplot of two pulse heights; see for example Fig. 5). In this way the relative numbers of protons, alphas and "others" in each of the selected bins were obtained. "Others" includes both good events of other low-Z species (mainly He-3) and also anomalous events with erroneous pulse heights corresponding to no identifiable species. Bins were grouped as "proton-rich" (more than 90 % protons) or "alpha-rich" (more than 90 % alpha particles). Bins not dominated by protons or alphas, or with a statistically insignificant event count, were discarded. In each range, for the proton-rich bin group, the "purity" (proton events in the bin group divided by total events in the bin group) and the "separated fraction" (proton events in the bin group divided by total proton events in all bins) were calculated. Corresponding calculations were done for the alpha-rich bin group. These results are summarized for each range in Table I.

For example, in range 0 (Fig. 2), the M2 - M1 plane can be partitioned into the bins defined above, e.g. the bin is 23 when the M2 channel number is in the range 16 - 32 and the M1 channel number is in the range 32 - 48. The same bin can occur in more than one place on the plot; for instance, the bin is also 23 if M2 is in the range 80 - 96 and/or if M1 is in the range 96 - 112. From Fig. 2 it can be seen that most protons fall in bin 33, with a smaller number in bins such as 23 and 32. Some alpha particles also fall in bin 33, but the protons predominate so this bin would be classed as proton-rich. On the other hand, bin 11 contains only alpha particles and would be classed as alpha-rich.

In all ranges except range 1, the PHA1 vs. PHA2 plot was always the plot used to define the species under consideration for event counting, by means of the boxes surrounding the tracks. In range 1, the D1 vs. M1 (PHA1 vs. PHA3) plot was used instead, on account of complications introduced by the M2 pulse height anomaly (described in section III). In this range, plots of PHA1 vs. PHA2 and PHA2 vs. PHA3 were useful in conjunction with PHA1 vs. PHA3 for characterizing and explaining the anomaly, as well as for selecting which of the many bins needed to be considered for further analysis.

Data from the time period 1978:266:0000 to 1978:271:0540 (a large solar flare) was used to obtain good statistics for both types of particles. Figs. 2, 3, 4, 5, and 6 are plots of this data for ranges 0, 1, 2, 3 and 4 respectively. (The pulse heights are of course integers; in these and other scatter plots contained in this report, the pulse heights plotted for each event have been displaced from the integral values by small random variables in order to better depict the density of events.) All events having the MH bit equal to zero were included; no other coincidence requirements were imposed. The events were not screened for satisfying the reduced geometry factor, because the statistics are a factor of three better with the large geometry factor and test runs indicated that the two geometry factors produce only statistically insignificant differences in the distribution of events in the bins. In range 0, the events were required to satisfy a reduced projected radius in detector D1. This was to eliminate particles with energies higher than range 0 which follow trajectories that miss D1 and later detectors, thereby being recorded as range 0 events. Similarly, range 2 events were required to satisfy a reduced D3 radius. The dimensions and spacing of the detectors are such that these are the only two cases where such exceptional trajectories are possible.

The results obtained for each species, and for alpha particles especially, depend of course on the alpha-to-proton ratio of the data used in this analysis; the ratio can vary by orders of magnitude but is usually in the 1 - 10 % range. It was about average (2 - 3 %) during the indicated time period, so the purity and separated fraction obtained here for alpha particles should be considered typical. The bin groupings given in Table I were made allowing for the possibility of a different alpha-to-proton ratio, i.e. the bins listed as proton- or alpha-rich should remain so for any reasonable value of this ratio. Bins highly sensitive to the ratio were discarded.

The overall purity and separated fraction are also of course dependent on the criterion used for the purity of the individual bins. One could, for instance, impose a stricter bin purity requirement (say 95 instead of 90 %) and enhance the overall "purity" of the species, at the expense of reducing the "separated fraction".

In ranges 0 and 1, all of the available pulse heights were used to obtain the maximum possible separation of protons and alphas. In ranges 2, 3 and 4, only the first two digits defining the bin were used and the correct 2-digit bin groupings could be read directly off a PHA1 vs. PHA2 plot (Figs. 4, 5, 6) just as in range 0. Use of additional pulse heights could be carried out straightforwardly but was not attempted here because relatively clean separation was achieved with just two pulse heights and because the number of possible bins increases by a factor of four for each new pulse height introduced. Moreover, the number of these bins which are occupied by a given species increases just as rapidly when matrix detector pulse heights are introduced. The matrix detector channel number(s) are often low, due to incomplete charge collection when particles pass between strips of the detector or at its edges. Hence the corresponding bin digit may have several possible values. With such a large number of bins, the available flight data is inadequate for a statistically meaningful analysis in these higher ranges, especially for alpha particles.

Completely aside from problems of separation, the usefulness of range 4 data in measuring absolute or relative proton fluxes is limited by the fact that in range 4 the number of observable protons begins to decline, as the energy loss in M1 and/or M2 falls below those detectors' 300-keV threshold. Data from higher ranges would likewise be useless for this purpose, even if the instrument were still capable of returning it. The range 4 alpha particle data can of course still be used for other purposes, e.g. alpha particle energy spectrum calculations.

In ranges 0 and 1, where both matrix detectors were used in the analysis, the boxes surrounding each species track were extended from the track itself down toward the threshold energy of the matrix detector(s) as far as possible (Figs. 2, 3), since the pulse heights for these detectors frequently fall below the main track values for a given species, as noted above. This can be done less successfully in range 0 than in range 1, on account of the M2 pulse height anomaly (see section III). The alpha particle boxes of course had to exclude the proton box, so some alphas, whose low matrix detector pulse height(s) placed them in the proton region of the plot, had to be treated as protons. The number of such alphas is small compared to both the total number of protons and the total number of alphas in the given range, so the error introduced is negligible. The total number of alphas falling below the main track amounts to about 10 % of all alphas in range 1, somewhat more in range 0.

In range 0, if the MH = 0 requirement is not imposed, proton events also extend upward from the main track; this is a rate-dependent effect, very prominent in the flare data (Fig. 7) but absent from quiet-time data (Fig. 8). It is caused by the "pileup" of particles at detector M1 during high-flux periods, i.e. low-energy particles stopping in M1 at the same time as genuine range 0 events pass through, thus adding to the observed M1 energy loss of the latter. These would also have to be included with the on-track protons, since although their number is always small compared to the on-track protons, it can be large compared to the number of below-track alphas in the same region. A large fraction of them are eliminated by requiring MH = 0 (Fig. 2), since usually the low-energy particle and the real range 0 particle will trigger non-adjacent strips or groups of strips in M1. This is the main reason for imposing the MH = 0 condition on the data to be analyzed; any absolute flux calculations would of course have to be corrected for the events discarded by this requirement. Relative fluxes are unaffected since the rate of occurrence of pileup is independent of range and geometry factor.

Pileup events can also be seen in data from range 1 if M1 is one of the pulse heights plotted (Figs. 3, 9).

If the usable bins listed in Table I are examined in conjunction with Figs. 2 - 6, 9 and 12, it is found that most or all of the protons and alpha particles in all energy intervals are identifiable, with the exception of the alpha particles in the extreme lower- and/or upper-energy parts of some ranges (the upper-left and lower-right sections of the "track"). These are lost due to ambiguities with the main proton track or with "others". For these cases we can define a truncated energy interval of interest, corresponding to just the unambiguous central segment of the track, and calculate the purity, separated fraction and "efficiency" for a modified grouping of bins which omits those corresponding to the already-poorly-represented end(s) of the track. These results appear in Table II. The bin groups have also been modified by lowering the purity requirement for the individual bins from 90 to 80 %. By comparing the Table II purity figures with those in Table I, it can be seen that this has a minor influence on the overall purity, while improving the coverage of the alpha track in some ranges. "Efficiency" is the total number of events in the bin group divided by the total number of events of the given species in all bins; thus "efficiency" is "separated fraction" divided by "purity", where "all bins" in these definitions now refers only to the bins comprising the usable energy interval.

Fig. 10 shows energy spectra averaged over the time period 1978:266:0000 to 1978:271:0540 for both protons and alpha particles, obtained by counting the number of identifiable low-Z particles in each range. The spectra are based on the results in Table II and each has been calculated in two ways: (1) using the original large geometry factor and nominal resolution of the instrument prior to the failure (the "HIST-I" mode) and (2) using the smaller geometry factor, reduced efficiencies and truncated energy intervals for alphas in some ranges which result from pulse height ambiguities in the degraded ("HIST-II") mode. The geometry factors were obtained from Ref. 5, or in the cases where reduced detector radii were used, from Ref. 6.

Fig. 11 is a plot of the ratio of the HIST-II flux to the HIST-I flux for each range and species. In the cases where the energy interval is different for the two fluxes, the ratio has been corrected for the energy spectrum obtained in Fig. 10 (a power law with spectral index of -2.2 for both species, although the correction is relatively insensitive to the exact spectral index used). There appear to be some systematic differences between the two methods of measuring the spectra. Averaged over energy, the HIST II/I ratio is (2.2 +/- 0.5) % low for protons and (9.4 +/- 3.3) % low for alpha particles; the values in the individual ranges indicate the presence of systematic errors of as much as 5 % for protons and 15 % for alphas. The error bars in Figs. 10 and 11 reflect only the statistical nature of the event counts; uncertainties in the calculated geometry factors and efficiencies are not included but are comparatively small.

Errors in the effective geometry factors are one possible explanation for the systematic lowness of the HIST II/I ratio. Another possibility is that the errors are an artifact of the "box" technique for distinguishing protons from alphas in pre-failure data. Redrawing the boxes somewhat differently, or defining them based on some other pulse height pair (or even on more than two pulse heights) might shed some light on the problem. The presence of pulse height anomalies, pileup, bit errors and the like complicate the process of defining events as protons or alphas. Note that all of these effects are unrelated to the readout failure and would have to be dealt with, although with less difficulty, in pre-failure data analysis as well.

The overall lowness of the alpha ratio relative to the proton ratio could be explained by a larger effective HIST-I geometry factor for alphas; in this model the matrix detector edges are more sensitive to alphas than to protons on account of the greater energy loss of the former. The effect is more important in the HIST-I mode because the matrix detector periphery is more irregular than in HIST-II.

III. ANOMALIES

In range 1, the PHA1 vs. PHA2 (D1 vs. M2) plot revealed a cluster of events just below the upper part of the alpha particle track, which did not correspond to a known species of particle (Fig. 12). They were interpreted as protons whose M2 pulse height was high by the amount of the M2 detector offset, since the group of events appeared directly above the proton track by this amount, about 33 channels. This hypothesis was supported by plots of D1 vs. M1 and M2 vs. M1. The abnormal events coincided with the proton track on D1 vs. M1 (Fig. 3), but their track was completely separate from both the proton and alpha tracks on M2 vs. M1, again displaced from the proton track by 33 channels along the M2-axis (Fig. 9). They also appear on PHA1 vs. PHA2 (M2 vs. M1) plots in range 0 (Fig. 2). The error in the M2 pulse height is thought to be due to the M2 ADC retriggering. The abnormal events appeared in the solar flare data, but not in quiet-time data (Figs. 13, 14, 15, 8), suggesting that the occurrence of bad M2 pulse heights is also a rate-dependent effect. By drawing a separate box around the bad events in range 1 (Fig. 12) and counting the number of events falling in the box each day, it was found that the occurrence of these events is correlated with the average low-Z range 1 rate for the corresponding day (Fig. 16). The reason for the apparent rate-dependence is not known. The uncertainties in the figure are actually higher than the purely statistical uncertainties indicated, especially at the low end of the rate scale, since the box also includes some below-track alpha particles. It can be seen from the figure that even at the highest daily rates measured, the bad-M2 protons amount to less than 5 % of all protons in range 1, and the fraction drops to less than 0.1 % at quiet periods. So overall, the exclusion of these events in range 1 would have a relatively small effect on the accuracy of proton numbers, but they can still be grouped with the normal protons anyway because their bins are distinct from those of alpha particles. If protons and alphas were defined by boxes on a D1 vs. M2 plot, the region of the plot where the bad events occur would have to be excluded from the alpha particle box, since the much higher abundance of protons over alphas ensures that even the bad protons may be comparable in number to alphas during flare periods. This exclusion would result in further loss of below-track alphas from the alpha box, but the problem can be avoided by defining the boxes in the D1 - M1 plane, where the anomaly does not appear. Since the anomalous events appear in the same place as normal protons on this plot, this ensures that all of the anomalous protons are treated as protons, and the only below-track alphas that are lost are those which fall on the main proton track. In range 0, the bad-M2 events cannot be distinguished from below-track alphas with only the two pulse heights, so they must be grouped with the normal protons, resulting in additional loss of below-track alphas in this range. In both ranges the bin-group choices in Table I take these anomalous events into account; this is unnecessary in the other ranges since the M2 pulse height, when available, is not used in the analysis.

In ranges 3 and 4, two small clusters of abnormal events were found, slightly displaced from the proton track on the PHA1 vs. PHA2 plot (Figs. 5 and 6, enlarged in Figs. 17 and 18). Since in both cases the displacement was along the D3-axis, and by about the same amount, these events were interpreted as protons whose D3 pulse heights were high by 8 or 12 channels. The effect is observed only over part of the proton track, when the normal D3 pulse height channel number is in the range 25 - 30. The error in the D3 pulse height is presumed due to some as yet unspecified electronics problem. The displacement of the track is small enough that the abnormal events fall into the same bins as normal protons, and they represent only a small fraction of the total number of protons anyway, so the anomaly has no effect on the accuracy of the proton count in ranges 3 and 4.

An examination of Figs. 2 - 6 also reveals several instances of events in clusters resembling the proton track in appearance but displaced along one of the axes by 16, 32 or 64 channels, usually downward into the region below the detector threshold. Examples are range 0 bin 13 (Fig. 2), range 1 bins 23 and 41 (Fig. 3) and range 2 bins 14 and 24 (Fig. 4). These are clearly protons with bit errors in one of the pulse heights. They constitute only a small fraction of the total protons (about 0.2 %) so their exclusion has a negligible effect on the accuracy of proton counts, but in a few cases they are ambiguous with alphas and comparable in number to the alphas in the same bin. In all other cases they could be grouped with the normal protons if desired.

In range 2 (Fig. 4), the proton track exhibits a "foldback" effect--a short track adjoining and extending below the main track. Such effects appear when trajectories for higher-energy particles are possible which miss the later detectors. As noted in section II, the events used in range 2 were restricted to a smaller projected D3 radius to eliminate this effect, so the reason for its persistence is not known. Possible explanations are a smaller-than-expected active area for D3 or a slight misalignment of the detectors.

IV. EXTENSION TO HIGH-Z NUCLEI

The approach and techniques developed above for separating protons and alpha particles can clearly be adapted to the problem of separating high-Z ($Z > 2$) species. This situation is more complicated on account of (1) a larger number of elements to be separated, (2) a larger number of useful bits available from each pulse height, and (3) lower elemental abundances resulting in fewer events observed, making a statistical analysis of flight data difficult. This section of the report will outline the situation with regard to high-Z separation, without attempting a comprehensive analysis of the problem.

The high-Z pulse height channel numbers extend all the way to the neighborhood of 4096, and the typical separation of adjacent element tracks on a PHA1 vs. PHA2 plot is about 100 channels, so the 256- and 512-bits now become important. In fact, these are by far the most important bits and as a first and simplest approximation, these bits alone were used, although the 16- and 32-bits were introduced later as a refinement. The 1- and 2-bits are again useless. One can now set up a system of bins based on the values of the 256- and 512-bits from each pulse height returned, analogous to the system established in section II for the 16- and 32-bits. One can again prepare PHA1 vs. PHA2 plots for ranges 0 through 4 (Figs. 19, 20, 21, 22, 23), partitioned according to the bin digits of the respective detectors.

These plots cover the entire time period before the instrument failure, including all data meeting the 16 x 16 matrix detector criterion; no other coincidence requirements have been imposed. It can be seen that in range 0 the elements C, N, O, Ne, Mg, Si, and Fe all appeared in statistically significant numbers, while in range 4 only C and O did. In view of the number of elements to be separated and the often inadequate statistics of the flight data, this entire problem was approached by means of a Monte Carlo computer simulation; the results could then be compared with analysis of flight data where statistics permit.

The computer program, written in FORTRAN, allowed a selected number of particles, distributed according to some chosen energy spectrum and set of relative abundances, to be incident on the HIST detector stack. The incidence angle was made to be a random variable distributed according to the actual angular distribution of the instrument. From the incident energy and angle of the particle, the known detector thicknesses and the range-energy relation, the particle's residual range before each detector could be determined; this in turn allowed calculation of the particle's residual energy before each detector and thus the energy loss in each. The energy losses were adjusted by a Gaussian random variable to represent detector thickness variation and Landau fluctuations. They were then converted to channel numbers using the energy calibration formula for the appropriate detector. The particle's "bin", as defined by the 256- and 512-bits of its pulse heights, was determined. For any given range, the program counted the number of particles of each species that fell into each bin, thus simulating the type of analysis done in section II on real data. In each bin, all isotopes of a given element were collected together. As before, the bins which were relatively "pure" in a given element could be grouped together, in order to calculate what fraction of the element could be resolved to within some minimum purity level, and over what energy intervals in each range this is possible.

The program was run using a power law energy spectrum with spectral index of -3 (-2 in range 4), and relative isotopic abundances for each element obtained from Cameron (Ref. 3). Relative elemental abundances used were also those given by Cameron, but modified by a Z-dependent "enhancement factor" deduced from the analysis of data from four earlier flares studied by Cook et al. (Ref. 4).

Tables III through VII summarize the results of the simulation for ranges 0 through 4. The tables list for each element its event total (out of 30,000 high-Z events altogether) and the percentage of the element that could be resolved to a purity of at least 100, 90, 80, 70 and 60 percent. Also given are composite percentages and event totals for certain groupings of elements: high abundance (C and O), medium abundance (N, Ne, Mg, Si and

Fe) and low abundance (all others); even-Z and odd-Z; and total high-Z. In ranges 0 and 1, the event totals for the elements were rescaled to improve statistics on the less abundant elements without increasing the total number of events to be simulated. Fig. 24 gives the energy intervals over which each even-high-Z element could be resolved to a purity of at least 80 %.

Attempts were made to improve these results by including some of the 16- and/or 32-bits in various combinations. Each additional bit used doubles the number of bins involved; the maximum number of bits used at one time is then set by practical limitations on the storage requirements and execution time of the simulation program. Within these limitations it was found that the 16- and 32-bits yielded little or no improvement over the results obtained using only the 256- and 512-bits, while greatly increasing the complexity of the analysis.

V. SEPARATION OF ISOTOPES

The FORTRAN program described above was modified for use in attempting to separate the isotopes of a given element. The elements considered were Ne and Mg, because (1) their elemental abundances are relatively high, (2) they each possess at least two isotopes with a relatively high isotopic abundance (about 10 % of the element or greater), and (3) they were found, by the analysis of section IV, to be relatively well-separated from other elements. On a PHA1 vs. PHA2 plot, the tracks of different isotopes of one element are separated by only about 10 channels, so it now becomes essential to use the 16- and 32- bits of the pulse heights. Using only the 256- and 512-bits, a "large bin" was selected which was both very pure in the desired element and contained a large fraction of the events of that element; isotopes of other elements were ignored from this point on. The large bin was then broken down into "small bins" based on the values of the 16- and 32-bits. The program counted the number of nuclei of each isotope that fell into each small bin.

It was found that for the large bins studied in detail, which represented the most favorable situations, it was not possible to get any significant separation of the isotopes to a purity approaching 90 %. However, the ratios between isotopes in individual small bins often differed significantly from the overall isotope ratio. So although actual event counts for each isotope could not be extracted from the data, it was still possible that the relative abundances of the isotopes could be inferred from the distribution of events among the small bins. When the simulation is repeated with different isotopic abundances, this distribution shifts. If the relative abundance of a particular isotope is increased, small bins rich in this isotope tend to acquire relatively more events, while bins poor in the isotope tend to acquire relatively fewer. In principle it might therefore be possible, by looking at the event totals in various groupings of small bins, to make a useful estimate of the overall isotope ratio in a particular data set. The drawback to this approach is that the number of events required, to obtain statistically meaningful event counts in the small bins, is larger than one could expect to obtain over the lifetime of the instrument.

A typical case is shown in Fig. 25. The calculations of section IV showed that "large bin" 22211 in range 3 is essentially pure Ne and contains a major fraction of the Ne in that range. This bin was subdivided into 16 "small bins" using the 16- and 32-bits from pulse heights D3 and D2 only. The isotopic composition of these bins was calculated using the following overall isotopic compositions:

Species	Composition Percentage #1	#2	#3
Ne-20	88.9	79.0	83.9
Ne-21	0.3	0.3	0.3
Ne-22	10.8	20.7	15.8

Composition #1 is the same as that given by Cameron. In Fig. 25, the small bins are ranked by their percentage content of Ne-22 for Compositions #1 and #2, with typical statistical error bars indicated. Note that while the overall Ne-22 percentage is 10.8 or 20.7, the percentage in individual bins ranges from near zero to about 50 %. By considering the statistical uncertainties present in various groupings of these bins, it was found that about 1100 Ne events in bin 22211 would be required to differentiate the two abundance patterns at a two-standard-deviation (95 %) confidence level. Since the results of section IV indicate that about 70 % of all range 3 Ne is in high-purity bins (see Table VI), the total number of range 3 Ne events required is about 1500, assuming that the other high-purity bins separate isotopes as well on the average as this one. If we assume that a comparable fraction of the Ne in other ranges is in high-purity bins (an overly optimistic assumption in view of Tables III-VII) and that these bins all separate the isotopes as well on the average as bin 22211 in range 3, then about 1500 total Ne events would be required. This can be pushed down to about 600-700 events by using the 16- and 32-bits of the other available pulse heights, while increasing the number of small bins to as many as 1024 (although only about 240 of these are ever occupied). Use of some of the 2-bits was attempted but this did not result in any consistent improvement.

The required event numbers above can be put into perspective by noting that the over three months of data preceding the instrument failure yielded only about 30 range 3 Ne events meeting the 16 x 16 matrix detector condition. During the 1978:266 solar flare, the largest flare observed prior to the failure, about 140 total Ne events were seen, with the original large geometry factor; the equivalent of about one additional flare of this magnitude was observed in the year following the failure. At least five such flares would be required to distinguish Compositions #1 and #2 -- not an unreasonable number given a high level of solar activity. However, the difference between these two Ne isotopic compositions is two or three times larger than what one could realistically expect to observe naturally (e.g. Cameron abundances vs. the solar wind Ne-22 abundance of about 7 %). The required event numbers would be at least an order of magnitude higher in the latter case, based on comparing the results of simulations using Compositions #1 and #3. Several other of the most promising Ne-rich large bins in various ranges were also analyzed in this way, as well as a few Mg-rich bins; these all yielded results comparable to or worse than those detailed above for one particular large bin. From all of this one can conclude that while useful information can still be extracted about the abundances of low-Z and even-high-Z elements, as described in earlier sections of this report, the situation with respect to isotope separation is somewhat doubtful.

It should be noted that the Monte-Carlo simulation program used throughout this work is not completely accurate, due mainly to inaccuracies in the detector thicknesses and range-energy relation that were used. However, although the results of the simulation may differ slightly in detail from actual data, the general results summarized here are considered valid. The thicknesses and range-energy relation used here are adequate for demonstration purposes, but if a program such as this were to be used in the actual analysis of flight data from the post-failure period, refinements would be necessary in these areas.

VI. REFERENCES

(1) ISEE Experiment Requirements Document, Heavy Isotope Spectrometer Telescope.

(2) Althouse, W. E., Cummings, A. C., Garrard, T. L., Mewaldt, R. A., Stone, E. C., and Vogt, R. E., Geosci. Electronics 16, 204 (1978).

(3) Cameron, A. G. W., Space Sci. Rev. 15, 121 (1970).

(4) Cook, W. R., Stone, E. C., and Vogt, R. E., Ap. J. (Letters) 238, L97 (1980).

(5) Mewaldt, R. A., SRL Internal Report #76 (1980).

(6) Mewaldt, R. A., private communication.

Table I. Separation of protons and alpha particles in ranges 0 through 4, based on data from the time period 1978:266:0000 to 1978:271:0540. All events meeting the MH = 0 condition have been included; no other coincidence requirements have been imposed. "Purity" is the number of events of the given species in the bin group divided by the total number of low-Z events in the bin group. "Separated fraction" is the number of events of the given species in the bin group divided by the total number of events of that species in all bins. Statistical uncertainties for these figures appear in parentheses. Bins used are all those which are at least 90 % pure in the given species, and are listed roughly in order of decreasing population.

Range	Pulse Heights Used	Species	Bins Used	Purity	Separated Fraction
0	M2,M1	proton	33,43,23,22	.999(.000)	.982(.001)
		alpha	11,21,42,31,41	.966(.006)	.693(.014)
1	D1,M2,M1	proton	433,133,423,432, 413,123,132,443, 422	.999(.000)	.996(.000)
		alpha	214,114,344,421, 121,124,314,213, 334,144,234,111, 343,411,313,141, 333,441,243	.974(.005)	.828(.011)
2	D2,D1	proton	44,14	.999(.000)	.999(.000)
		alpha	22,12,31,32,42	.986(.006)	.873(.015)
3	D3,D2	proton	24,34	1.000(.000)	.999(.000)
		alpha	32,11,41,42	.981(.007)	.860(.017)
4	D4,D3	proton	42,43,12,13	.998(.001)	1.000(.000)
		alpha	33,14,24,41,11	.972(.012)	.901(.022)

Table II. Usable energy intervals for protons and alpha particle identification in ranges 0 through 4, based on data from the time period 1978:266:0000 to 1978:271:0540. All events meeting the MH = 0 condition have been included; no other coincidence requirements have been imposed. Purity and separated fraction are as defined in Table I, but "all bins" now refers only to those bins comprising the usable energy interval. "Efficiency" is the number of events in the bin group divided by the total number of events of the given species in all bins, i.e. separated fraction divided by purity. Statistical uncertainties for these figures appear in parentheses. Bins are listed roughly in order of decreasing population. Bins in parentheses are of 80 - 90 % purity; all others are at least 90 % pure. HIST-I energy interval boundaries are given in parentheses where different from HIST-II.

Range	Pulse Heights Used	Species	Bins Used	Purity	Sep. Fract.	Efficiency	HIST-II Usable Energy Interval (MeV/nucleon)
0	M2,M1	proton	33,43,23,22	.999 (.000)	.982 (.001)	.983 (.001)	2.309 - 3.224
		alpha	11,21,42,31, 41,(14,44, 12,24)	.949 (.007)	.986 (.004)	1.039 (.007)	2.272 - 3.111 (2.193)
1	D1,M2,M1	proton	433,133,423, 432,413,123, 132,(434), 443,422	.999 (.000)	.997 (.000)	.998 (.000)	3.224 - 4.784
		alpha	214,114,344, 121,124,314, 213,334,144, 234,111,343, 313,141,333, 243	.975 (.005)	.865 (.010)	.887 (.011)	3.215 - 4.659 (3.111)
2	D2,D1	proton	44,14	.999 (.000)	.999 (.000)	.999 (.000)	4.784 - 6.889
		alpha	22,12,31, (43),32,42	.969 (.008)	.979 (.007)	1.011 (.005)	4.659 - 6.612
3	D3,D2	proton	24,34	1.000 (.000)	.999 (.000)	.999 (.000)	6.889 - 11.84
		alpha	32,11,41,42	.981 (.007)	1.000 (.000)	1.019 (.007)	6.833 - 10.97 (6.612) (11.33)
4	D4,D3	proton	42,43,12,13	.998 (.001)	1.000 (.000)	1.002 (.001)	11.84 - 20.93
		alpha	33,14,24, 41,(23),11	.954 (.015)	.979 (.010)	1.026 (.012)	11.33 - 20.41

Table III. Percentage of high-Z elements that can be separated to various levels of purity in range 0, using only the 256- and 512-bits of the pulse height channel numbers. These are results of a Monte Carlo computer calculation. A power-law energy spectrum with spectral index of -3 was assumed; elemental abundances are those given by Cameron (Ref. 3). "Total events" reflects the assumed abundances of the elements; "scaled events" is the actual number of events simulated, to improve statistics on the less abundant elements. "High" abundance refers to C and O; "medium" is N, Ne, Mg, Si, and Fe; "low" is all others.

Z	100 %	90 %	80 %	70 %	60 %	TOTAL EVENTS	SCALED EVENTS
6	0.0	0.0	56.0623	65.9888	65.9888	8826.0977	5023
7	0.0	0.0	0.0	0.0	0.0	1834.1284	2462
8	0.0	55.6599	55.6599	55.6599	55.6599	13594.6484	6743
9	0.0	0.0	0.0	0.0	0.0	1.4189	65
10	0.0	0.0	29.5910	29.5910	29.5910	1641.8386	2924
11	0.0	0.0	0.0	0.0	0.0	122.5228	600
12	0.0	0.0	38.6011	38.6011	38.6011	1803.7148	3570
13	0.0	0.0	0.0	0.0	0.0	116.4948	595
14	0.0	0.0	0.0	10.9475	27.8490	1109.2708	2458
15	0.0	0.0	0.0	0.0	0.0	7.1154	145
16	0.0	0.0	0.0	0.0	0.0	202.3299	982
17	0.0	0.0	0.0	0.0	0.0	1.3221	62
18	0.0	0.0	0.0	0.0	0.0	22.4429	339
19	0.0	0.0	0.0	0.0	0.0	2.2065	80
20	0.0	0.0	0.0	0.0	0.0	62.7355	490
22	0.0	0.0	0.0	0.0	0.0	1.8425	74
24	0.0	0.0	0.0	0.0	0.0	9.8293	216
25	0.0	0.0	0.0	0.0	0.0	7.3396	147
26	0.0	0.0	0.0	0.0	0.0	595.5291	1855
27	0.0	0.0	0.0	0.0	0.0	1.6705	70
28	0.0	0.0	0.0	0.0	0.0	35.5534	502
LOW	0.0	0.0	0.0	0.0	0.0	594.8228	4357
MED	0.0	0.0	16.9245	18.6632	21.3475	6984.4766	13279
HIGH	0.0	33.7490	55.8183	59.7260	59.7260	22420.7461	12366
EVEN	0.0	27.1154	49.0828	52.6576	53.3294	27905.8164	25786
ODD	0.0	0.0	0.0	0.0	0.0	2094.2180	4218
TOTL	0.0	25.2227	45.6567	48.9819	49.6069	29999.9023	30002

Table IV. Percentage of high-Z elements that can be separated to various levels of purity in range 1, using only the 256- and 512-bits of the pulse height channel numbers. These are results of a Monte Carlo computer calculation. A power-law energy spectrum with spectral index of -3 was assumed; elemental abundances are those given by Cameron (Ref. 3).

Z	100 %	90 %	80 %	70 %	60 %	TOTAL EVENTS	SCALED EVENTS
6	0.0	99.9099	99.9099	99.9099	99.9099	8811.2969	5618
7	0.0	39.7724	39.7724	39.7724	39.7724	1833.7783	2462
8	0.0	76.9414	76.9414	96.1509	96.1509	13607.6563	6748
9	0.0	0.0	0.0	0.0	0.0	1.4188	65
10	0.0	53.1431	53.1431	53.1431	53.1431	1643.8777	2936
11	0.0	8.3330	8.3330	8.3330	8.3330	122.5708	600
12	0.0	42.3644	85.3388	88.0950	93.2618	1805.5251	3572
13	0.0	0.0	0.0	7.0081	7.0081	116.5229	585
14	0.0	38.0384	57.4512	91.9712	91.9712	1110.1711	2459
15	0.0	0.0	0.0	0.0	0.0	7.1148	145
16	0.0	0.0	0.0	0.0	25.2679	202.4348	982
17	0.0	0.0	0.0	0.0	0.0	1.3213	62
18	0.0	0.0	0.0	0.0	10.7962	22.4442	339
19	0.0	0.0	0.0	0.0	0.0	2.2063	81
20	0.0	2.4450	21.3464	31.8511	39.6281	62.7055	490
22	0.0	4.0840	4.0840	4.0840	4.0840	1.8370	73
24	0.0	0.0	0.0	0.0	0.0	9.7945	216
25	0.0	0.0	0.0	0.0	0.0	7.3068	147
26	0.0	18.8329	36.3996	45.8563	46.3825	593.0698	1852
27	0.0	0.0	0.0	0.0	0.0	1.6023	70
28	0.0	0.0	5.4780	11.3299	11.3299	35.3777	530
LOW	0.0	1.9378	4.3066	7.1354	16.9637	594.7166	4355
MED	0.0	41.5353	57.2173	64.2177	65.5977	6986.4141	13281
HIGH	0.0	85.9687	85.9687	97.6282	97.6282	22418.9531	12366
EVEN	0.0	76.8553	80.8306	91.9813	92.5362	27906.1680	25785
ODD	0.0	35.3193	35.3193	35.7093	35.7093	2093.9019	4217
TOTL	0.0	73.9553	77.6533	88.0527	88.5689	30000.4180	30002

Table V. Percentage of high-Z elements that can be separated to various levels of purity in range 2, using only the 256- and 512-bits of the pulse height channel numbers. These are results of a Monte Carlo computer calculation. A power-law energy spectrum with spectral index of -3 was assumed; elemental abundances are those given by Cameron (Ref. 3).

Z	100 %	90 %	80 %	70 %	60 %	TOTAL EVENTS
6	0.0	23.5207	60.4347	100.0000	100.0000	8788
7	0.0	0.0	0.0	0.0	0.0	1833
8	24.6750	96.1151	97.3783	97.3783	97.3783	13617
9	0.0	0.0	0.0	0.0	0.0	1
10	0.0	60.8379	60.8379	60.8379	60.8379	1647
11	0.0	0.0	0.0	0.0	0.0	123
12	0.0	65.5077	66.7218	66.7218	92.7152	1812
13	0.0	0.0	0.0	0.0	0.0	117
14	0.0	61.4901	72.9802	73.8779	73.8779	1114
15	28.5714	28.5714	28.5714	28.5714	28.5714	7
16	29.5566	55.1724	69.4581	84.7290	84.7290	203
17	0.0	0.0	0.0	0.0	0.0	1
18	60.8696	60.8696	60.8696	60.8696	78.2609	23
19	0.0	0.0	0.0	0.0	0.0	2
20	83.8710	83.8710	83.8710	95.1613	95.1613	62
22	0.0	0.0	0.0	0.0	0.0	2
24	30.0000	30.0000	30.0000	30.0000	30.0000	10
25	0.0	0.0	0.0	0.0	0.0	7
26	39.6290	65.5986	71.1636	71.1636	71.8331	593
27	0.0	0.0	0.0	0.0	0.0	2
28	8.5714	8.5714	20.0000	20.0000	20.0000	35
	12.4304	62.0154	74.1225	85.8728	87.4696	29999
C, O	14.9967	67.6412	82.8877	98.4066	98.4066	22405
N, Ne, Mg, Si, Fe	3.3576	46.6207	49.2356	49.5785	56.1652	6999
OTHER	22.5210	31.2605	36.8067	43.1933	43.8655	595

Table VI. Percentage of high-Z elements that can be separated to various levels of purity in range 3, using only the 256- and 512-bits of the pulse height channel numbers. These are results of a Monte Carlo computer calculation. A power-law energy spectrum with spectral index of -3 was assumed; elemental abundances are those given by Cameron (Ref. 3).

Z	100 %	90 %	80 %	70 %	60 %	TOTAL EVENTS
6	0.0	49.8175	49.8175	49.8175	49.8175	8766
7	0.0	0.0	0.0	0.0	0.0	1831
8	3.9639	40.9234	40.9234	40.9234	79.5199	13623
9	0.0	0.0	0.0	0.0	0.0	1
10	34.7273	72.7879	72.7879	72.7879	94.1212	1650
11	0.0	0.0	0.0	0.0	16.2602	123
12	6.6043	38.4700	83.8195	83.8195	89.3231	1817
13	0.0	0.0	0.0	6.8376	6.8376	117
14	10.1073	33.5420	88.9982	88.9982	88.9982	1118
15	28.5714	28.5714	28.5714	28.5714	28.5714	7
16	32.8431	56.3725	56.3725	56.3725	57.3529	204
17	0.0	0.0	0.0	0.0	0.0	1
18	60.8696	60.8696	60.8696	60.8696	60.8696	23
19	0.0	0.0	0.0	0.0	0.0	2
20	79.3651	79.3651	79.3651	79.3651	85.7143	63
22	0.0	0.0	0.0	0.0	0.0	2
24	20.0000	20.0000	20.0000	20.0000	20.0000	10
25	14.2857	14.2857	14.2857	14.2857	14.2857	7
26	42.7609	76.5993	87.5421	88.5522	88.5522	594
27	0.0	0.0	0.0	0.0	0.0	2
28	42.8571	42.8571	42.8571	42.8571	48.5714	35
LOW	25.2931	33.3333	33.3333	34.6734	39.3635	597
MED	15.1213	38.9444	60.4707	60.5563	67.0043	7010
HIGH	2.4119	44.4057	44.4057	44.4057	67.8905	22389
EVEN	6.2641	46.1136	51.5212	51.5427	72.0337	27905
ODD	0.1435	0.1435	0.1435	0.5261	1.4825	2091
TOTL	5.8374	42.9090	47.9397	47.9864	67.1156	29996

Table VII. Percentage of high-Z elements that can be separated to various levels of purity in range 4, using only the 256- and 512-bits of the pulse height channel numbers. These are results of a Monte Carlo computer calculation. A power-law energy spectrum with spectral index of -2 was assumed; elemental abundances are those given by Cameron (Ref. 3).

Z	100 %	90 %	80 %	70 %	60 %	TOTAL EVENTS
6	0.0	46.0311	46.0311	46.0311	46.0311	7332
7	0.0	0.0	0.0	0.0	0.0	1674
8	11.8679	11.8679	37.0984	71.2820	71.2820	13448
9	0.0	0.0	0.0	0.0	0.0	1
10	0.8161	18.6616	52.7203	52.7203	52.7203	1838
11	0.0	0.0	4.9296	4.9296	4.9296	142
12	0.0	55.9322	83.4077	83.4077	92.5067	2242
13	0.0	0.0	0.0	10.0671	11.4094	149
14	0.0	85.8086	89.5049	89.5049	98.2838	1515
15	0.0	0.0	0.0	0.0	0.0	10
16	13.0872	34.8993	47.6510	64.0939	64.0939	298
17	0.0	0.0	0.0	0.0	0.0	2
18	11.4286	11.4286	11.4286	11.4286	17.1429	35
19	0.0	0.0	0.0	0.0	0.0	4
20	43.2692	43.2692	43.2692	43.2692	43.2692	104
22	33.3333	33.3333	33.3333	33.3333	33.3333	3
24	0.0	0.0	0.0	0.0	0.0	17
25	7.6923	7.6923	7.6923	7.6923	7.6923	13
26	31.5406	79.7630	94.1659	96.1714	97.9945	1097
27	0.0	0.0	0.0	0.0	0.0	3
28	28.5714	28.5714	35.7143	40.0000	40.0000	70
LOW	12.9260	20.5640	26.4395	34.3126	34.7826	851
MED	4.3151	45.0872	62.4910	62.7540	67.0213	8366
HIGH	7.6805	23.9220	40.2502	62.3725	62.3725	20780
EVEN	7.3788	31.8476	49.3196	66.0023	67.2845	27999
ODD	0.0501	0.0501	0.4004	1.1512	1.2513	1998
TOTL	6.8907	29.7296	46.0613	61.6828	62.8863	29997

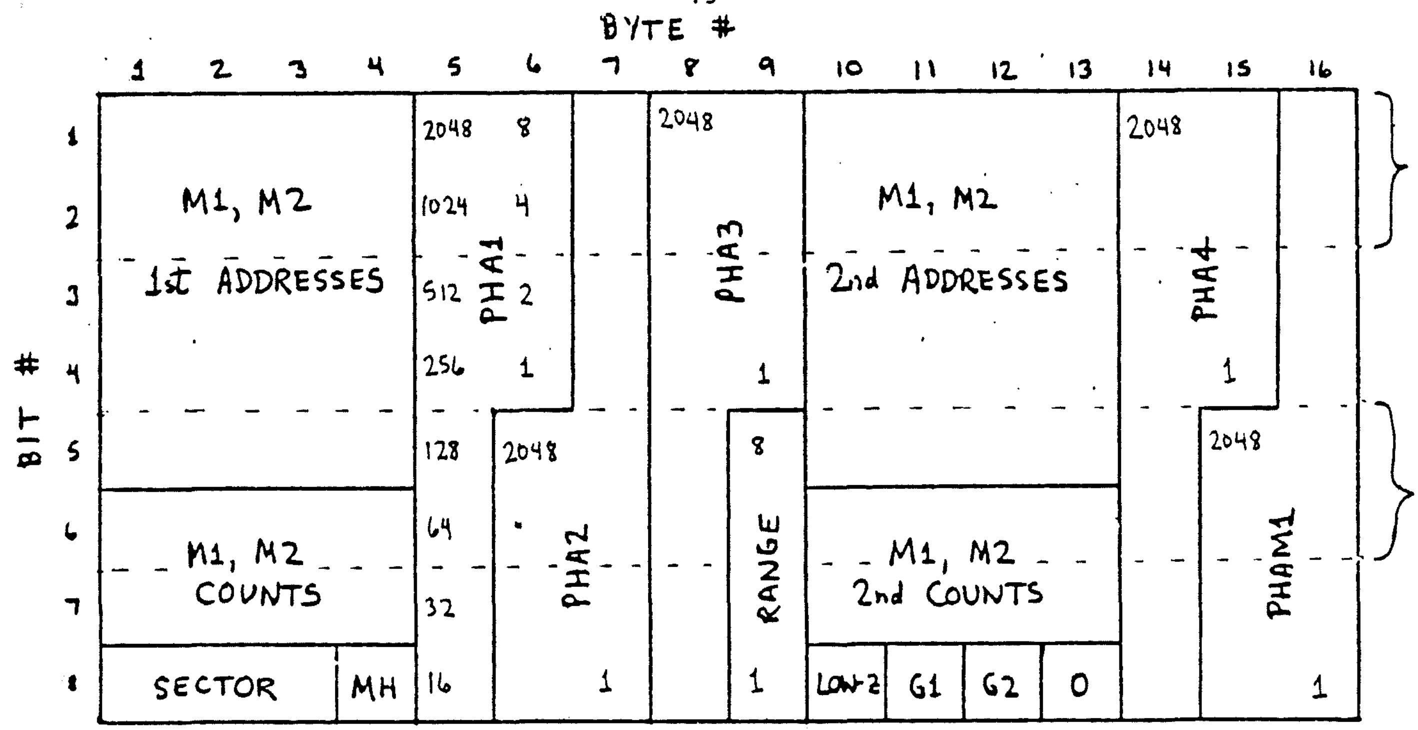

Figure 1. HIST event data format. Rows of bits within brackets (#1, 2, 5, 6) are presently lost. See Ref. 1 for more information.

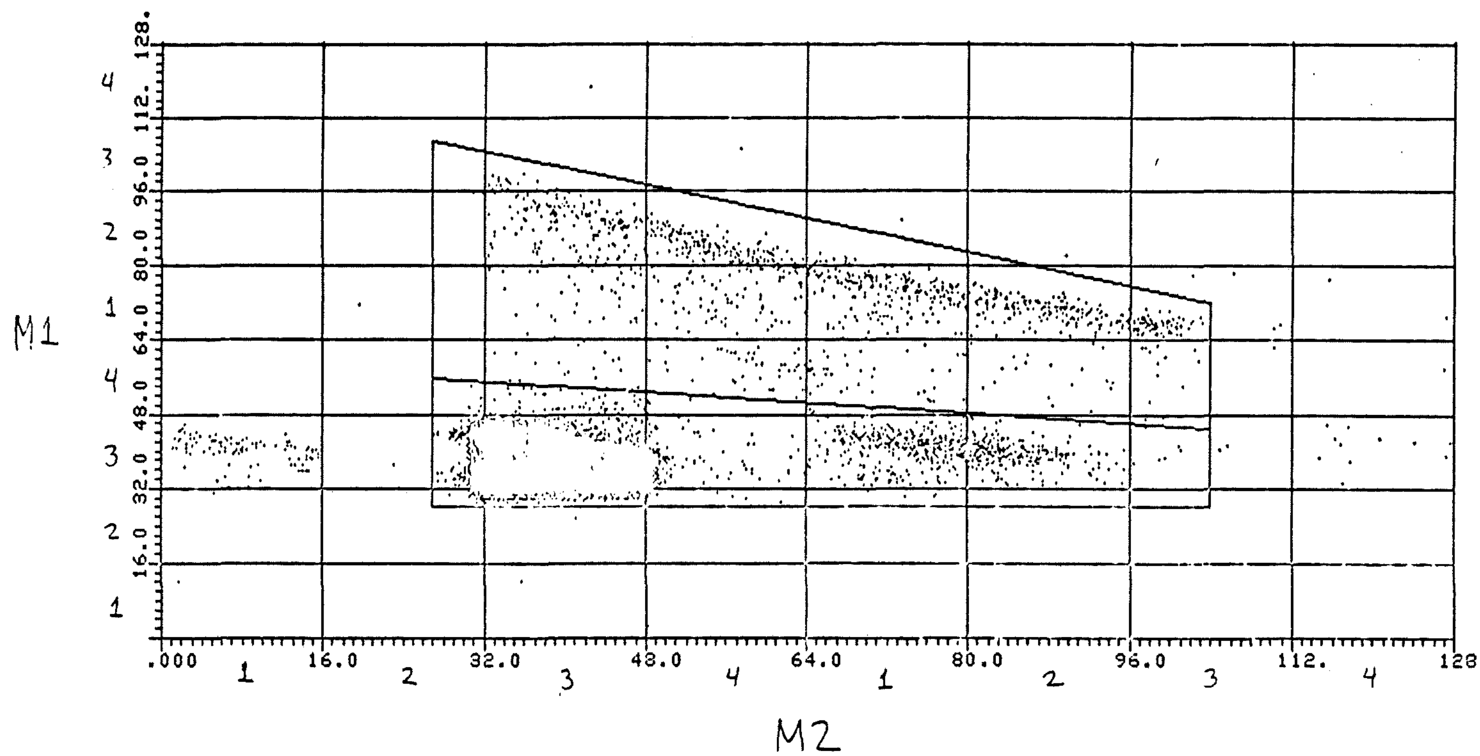

Figure 2. M2 vs. M1 (PHA1 vs. PHA2) plot of range 0 low-Z data from the time period 1978:266:0000 to 1978:271:0540. All events with MH (multiple hodo) bit equal to zero are included. Note boxes surrounding element tracks and "bin" digits denoting values of the 16- and 32-channel pulse height bits. Also note anomalous protons with bad M2 pulse heights (bins 13, 23).

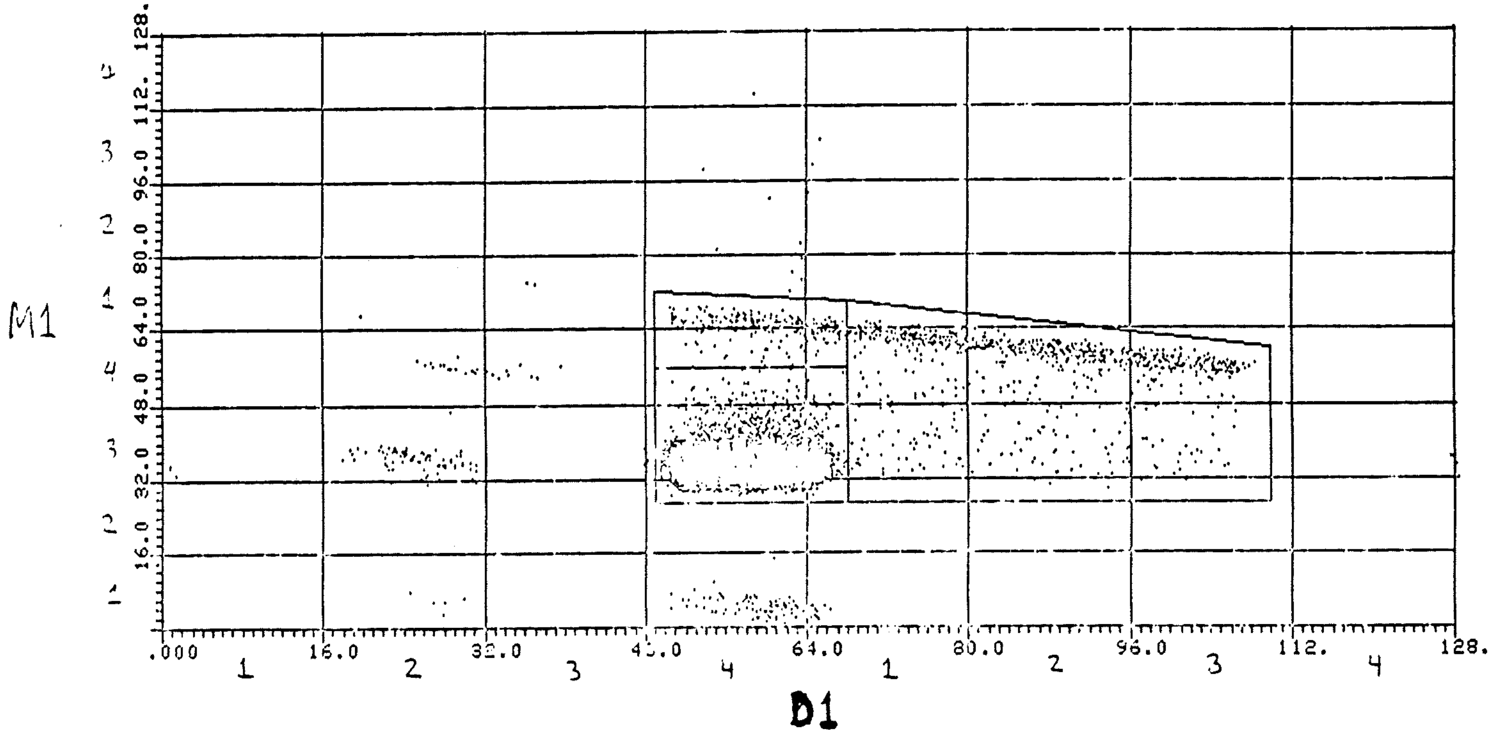

Figure 3. D1 vs. M1 (PHA1 vs. PHA3) plot of range 1 low-Z data from the time period 1978:266:0000 to 1978:271:0540, including events with MH = 0 only. Lower track consists of both normal protons and anomalous proton events with bad M2 pulse heights. Note clusters of protons with pulse height bit errors (bins 41, 23).

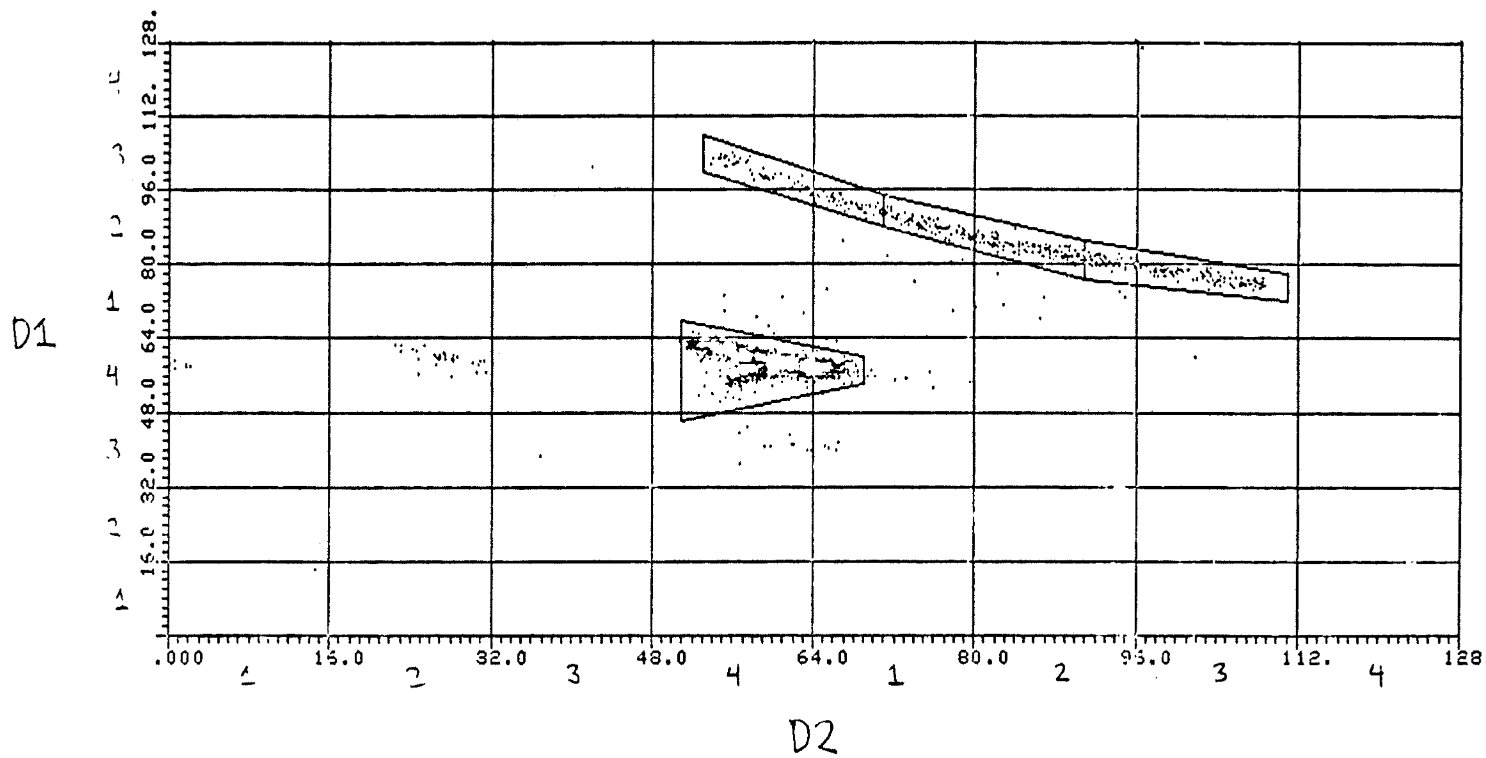

Figure 4. D2 vs. D1 (PHA1 vs. PHA2) plot of range 2 low-Z data from the time period 1978:266:0000 to 1978:271:0540, including events with MH = 0 only. Note cluster of protons with pulse height bit error (bin 24). Note also the "foldback" of protons below the main track.

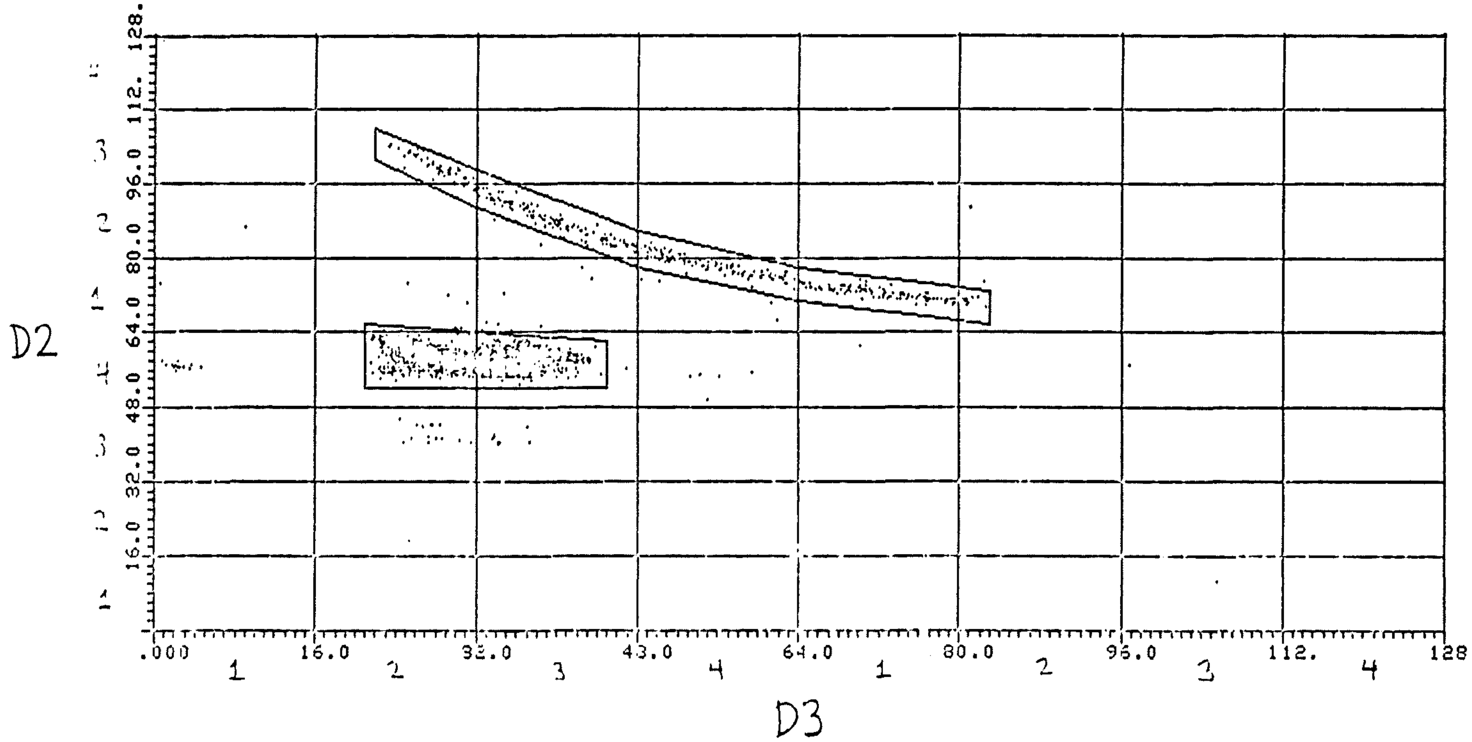

Figure 5. D3 vs. D2 (PHA1 vs. PHA2) plot of range 3 low-Z data from the time period 1978:266:0000 to 1978:271:0540, including events with MH = 0 only. Note anomalous proton events near main track.

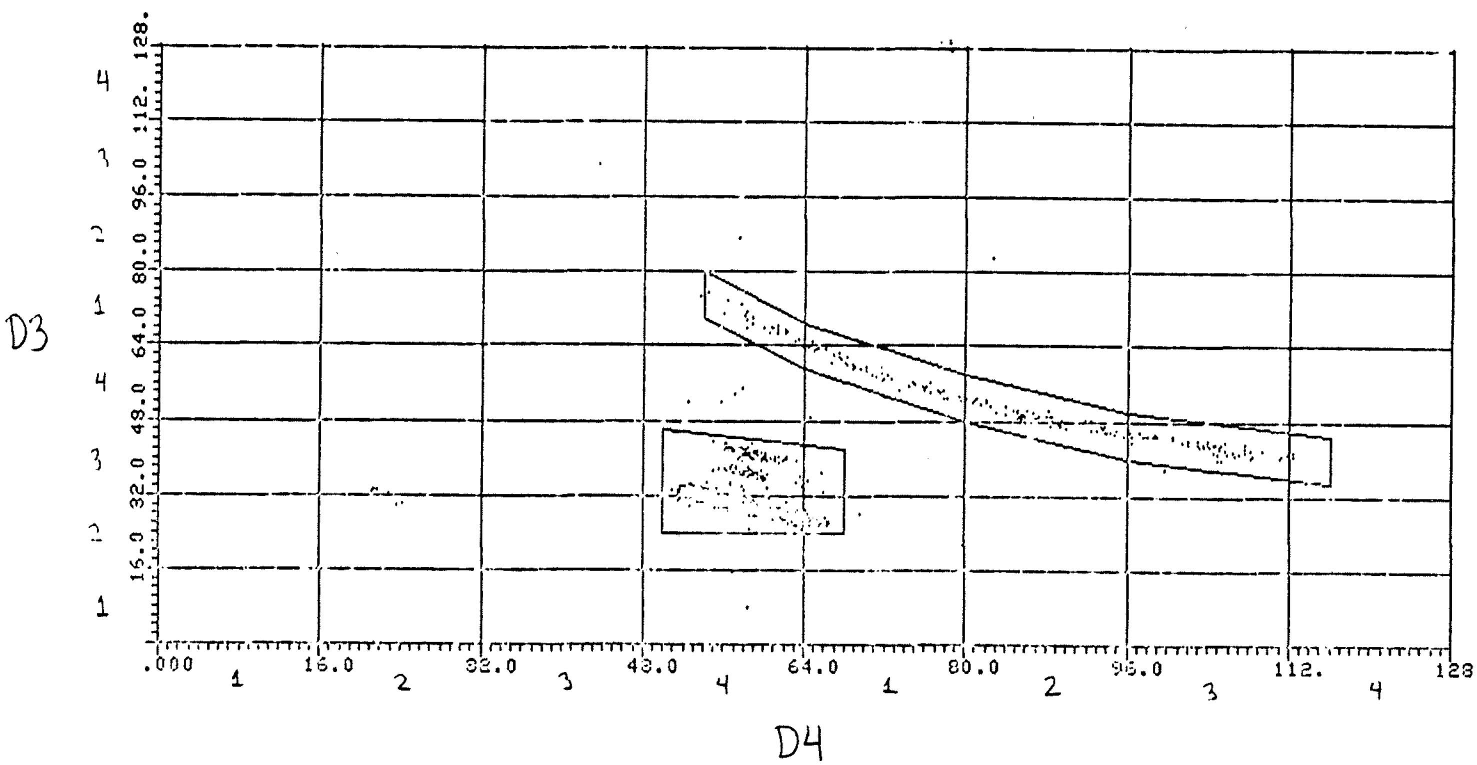

Figure 6. D4 vs. D3 (PHA1 vs. PHA2) plot of range 4 low-Z data from the time period 1978:266:0000 to 1978:271:0540, including events with MH = 0 only. Note anomalous proton events near main track.

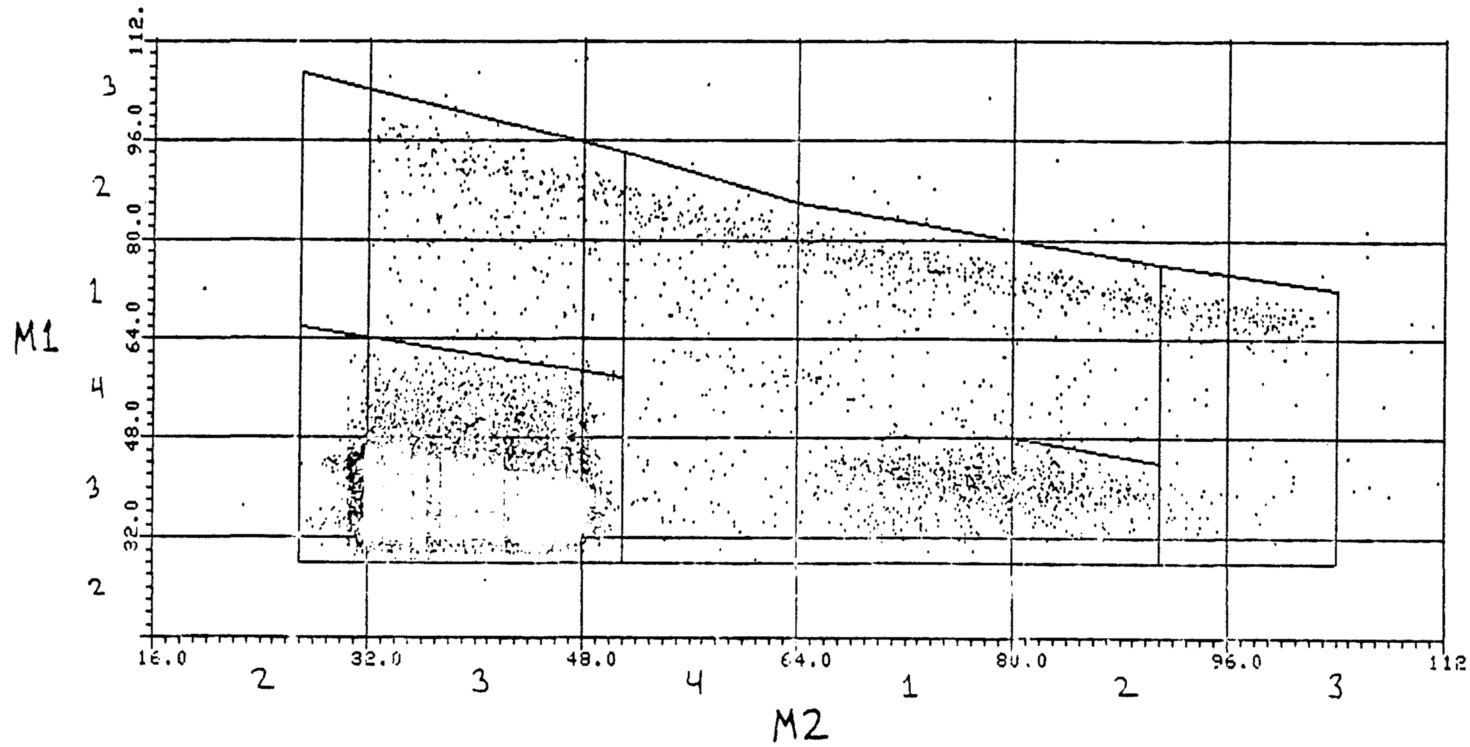

Figure 7. M2 vs. M1 (PHA1 vs. PHA2) plot of range 0 low-Z data from the time period 1978:267-271, with MH bit unspecified. Note protons with bad M2 pulse heights (bins 13, 23) and "pileup" events above main proton track.

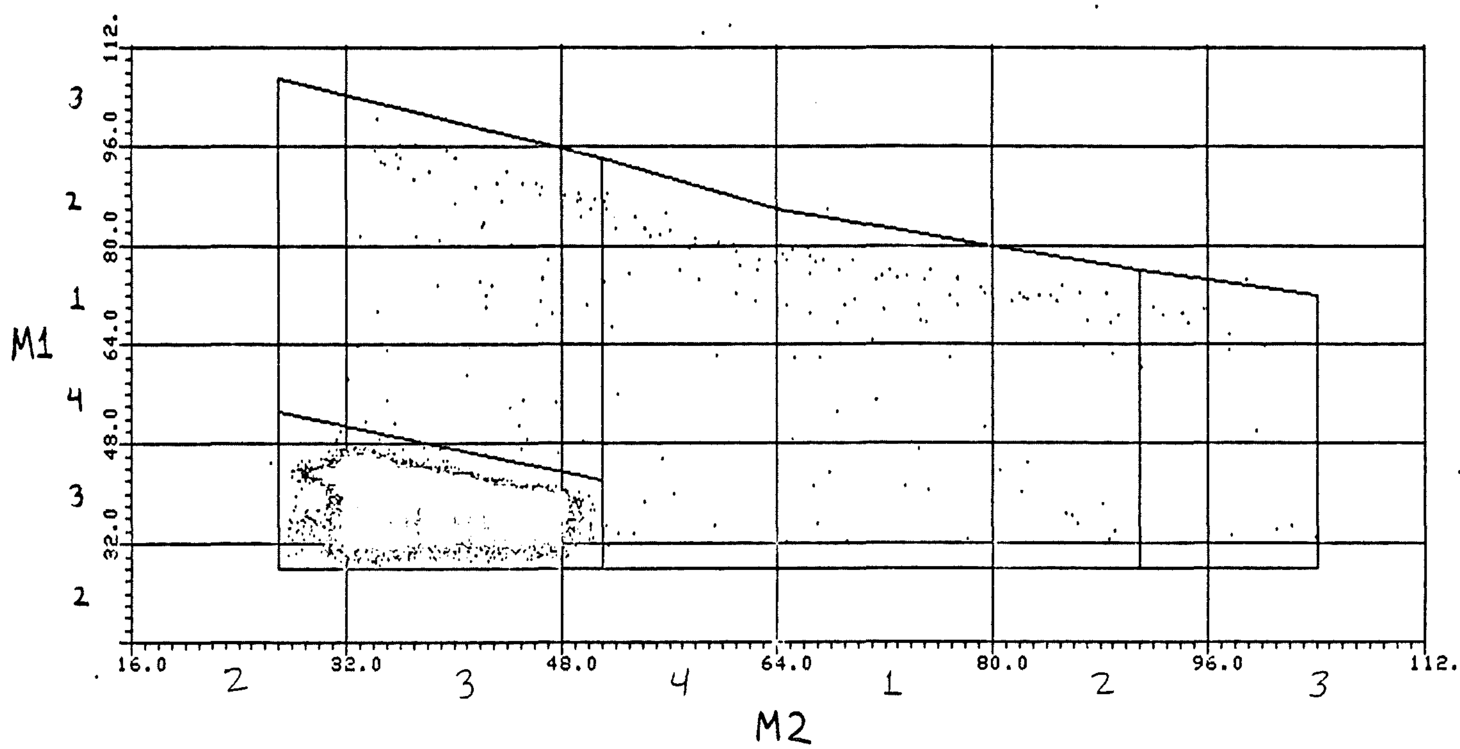

Figure 8. M2 vs. M1 (PHA1 vs. PHA2) plot of range 0 low-Z data from the time period 1978:226-265, with MH bit unspecified. "Pileup" and bad-M2 protons are absent.

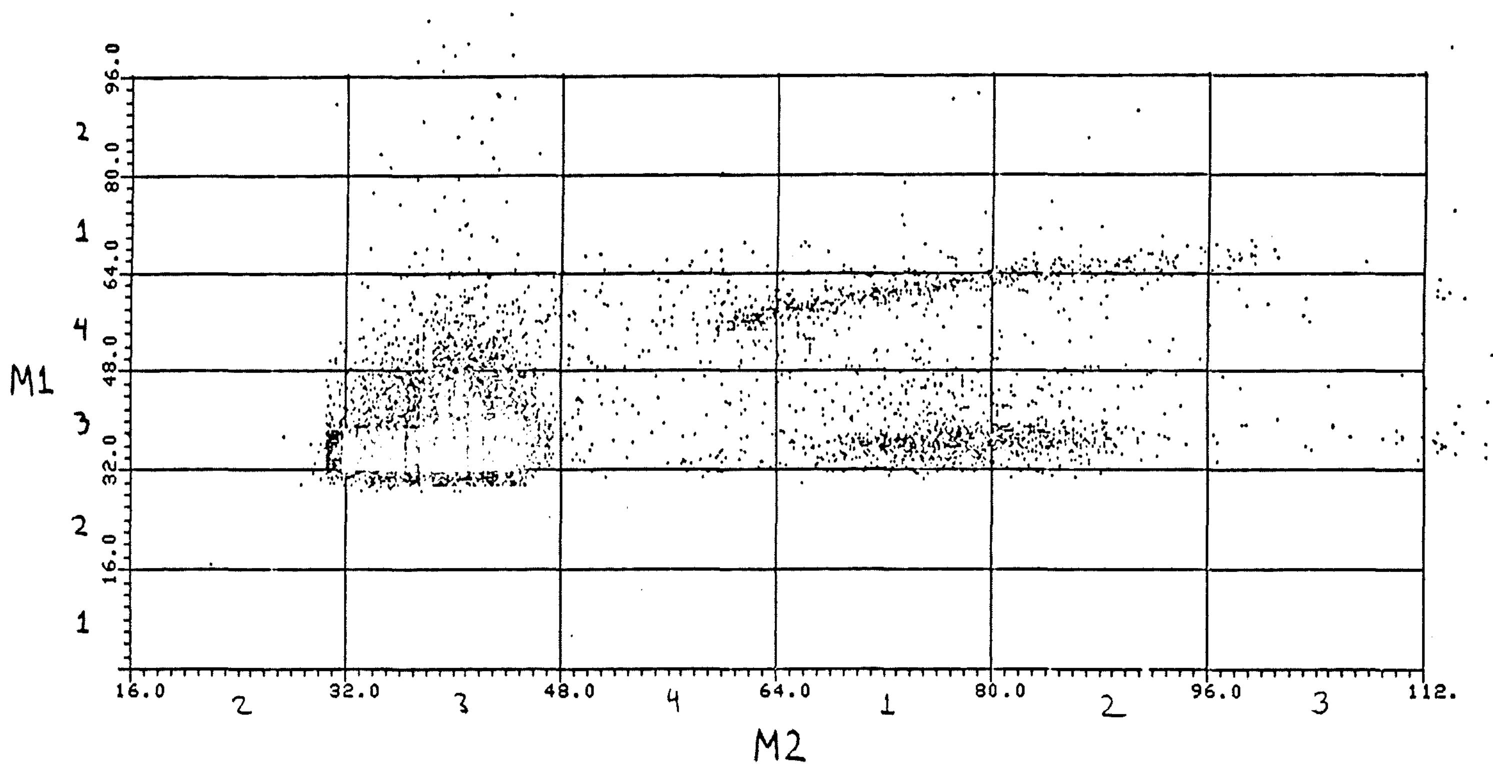

Figure 9. M2 vs. M1 (PHA2 vs. PHA3) plot of range 1 low-Z data from the time period 1978:267-271, with MH bit unspecified. Note anomalous proton events with bad M2 pulse heights (bins 13, 23) and "pileup" events above main proton track.

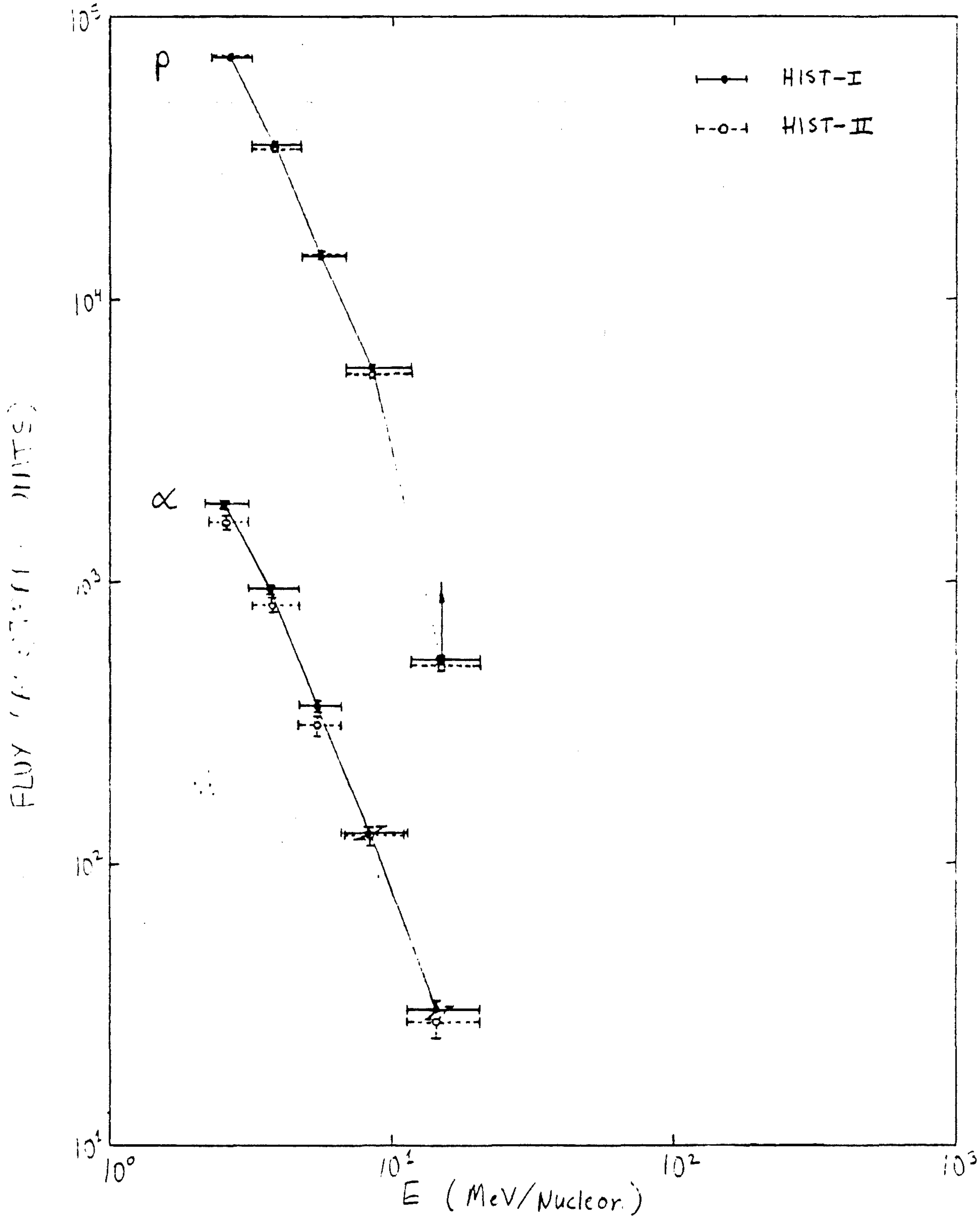

Figure 10. Energy spectra averaged over the time period 1978:266:0000 to 1978:271:0540 (solar flare) for both protons and alpha particles; calculated using both the original large geometry factor and nominal resolution (HIST-I) and using the reduced geometry factor, reduced efficiencies and truncated energy intervals present in the degraded (HIST-II) mode.

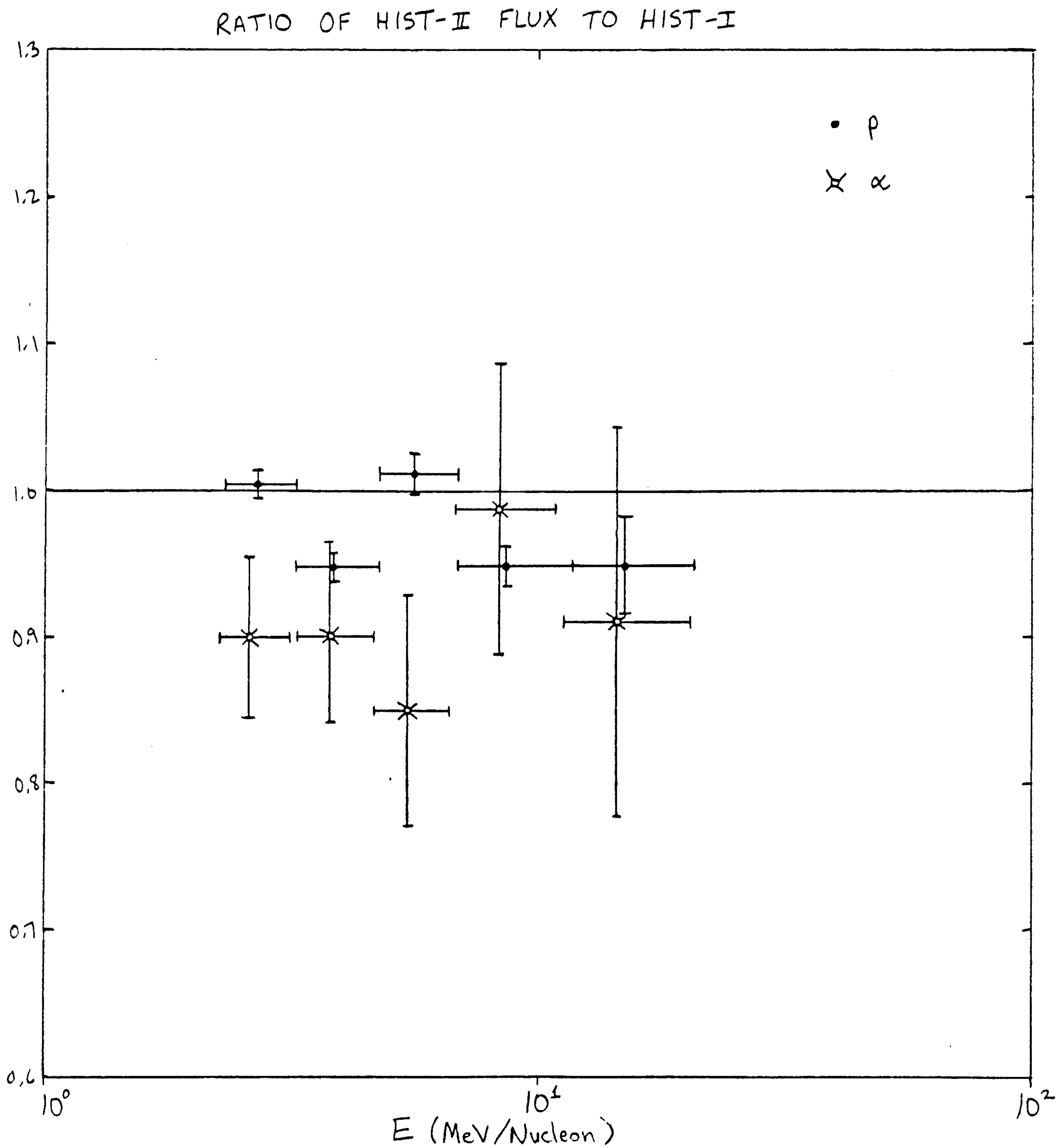

Figure 11. Ratio of the HIST-II flux to HIST-I flux averaged over the time period 1978:266:0000 to 1978:271:0540, for each range for both protons and alpha particles.

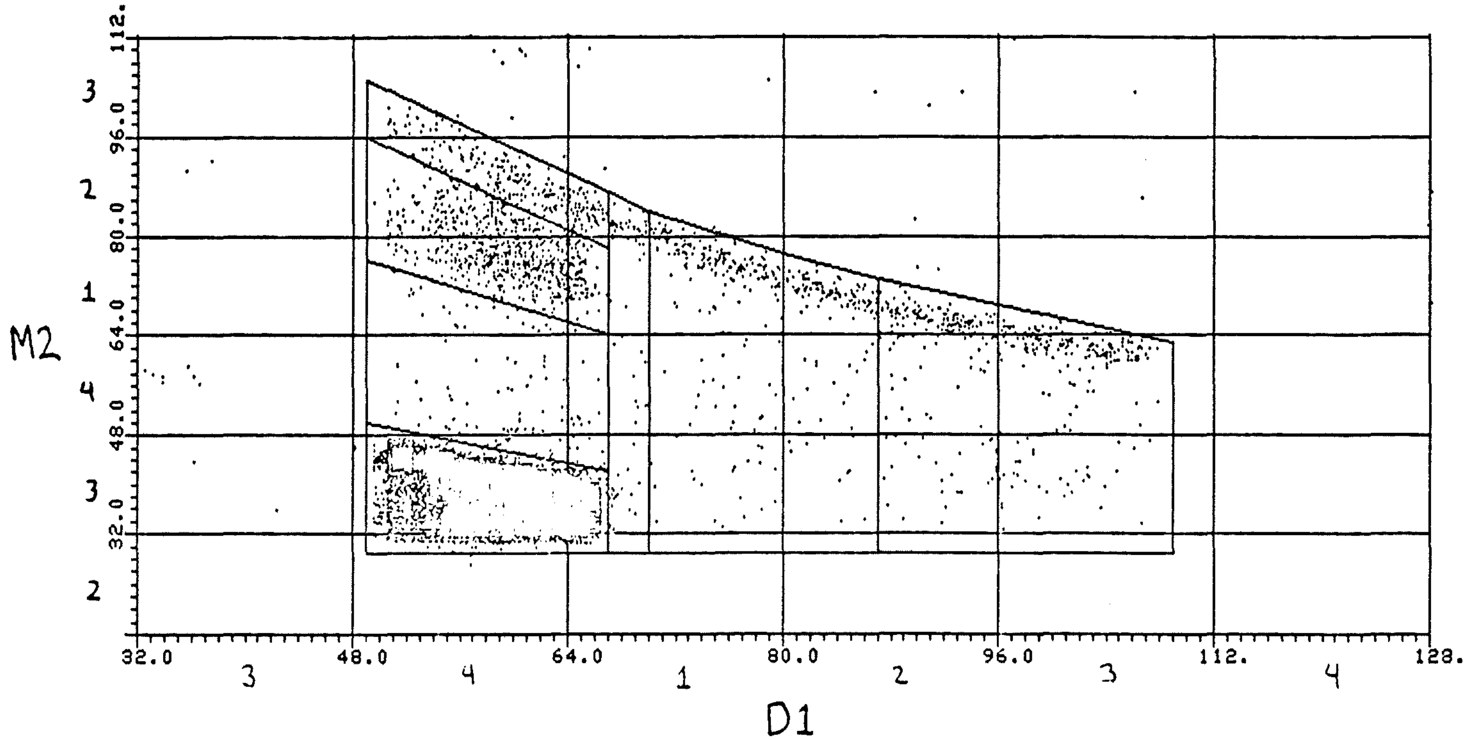

Figure 12. D1 vs. M2 (PHA1 vs. PHA2) plot of range 1 low-Z data from the time period 1978:267-271. Note bad-M2 proton cluster displaced about 33 channels above main proton track.

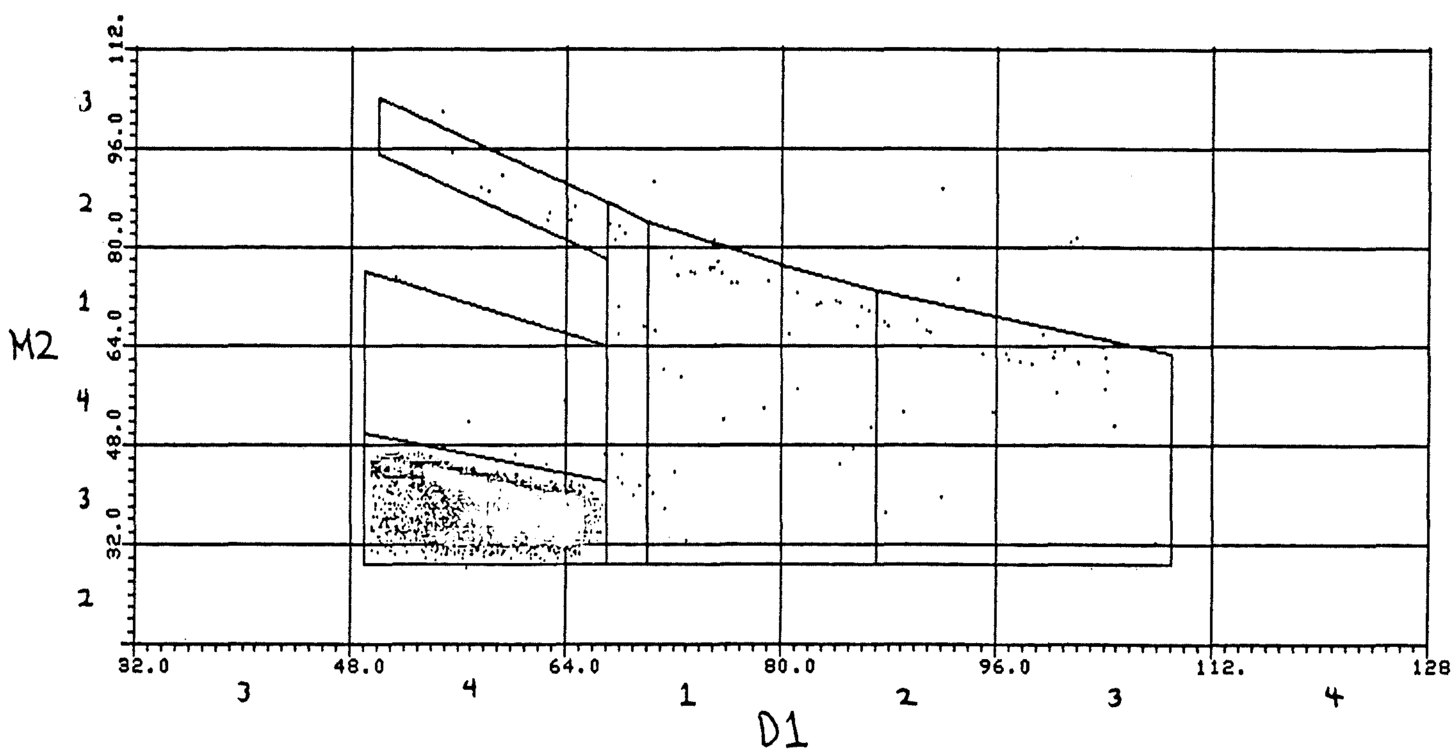

Figure 13. D1 vs. M2 (PHA1 vs. PHA2) plot of range 1 low-Z data from the time period 1978:226-265. Bad-M2 protons are absent.

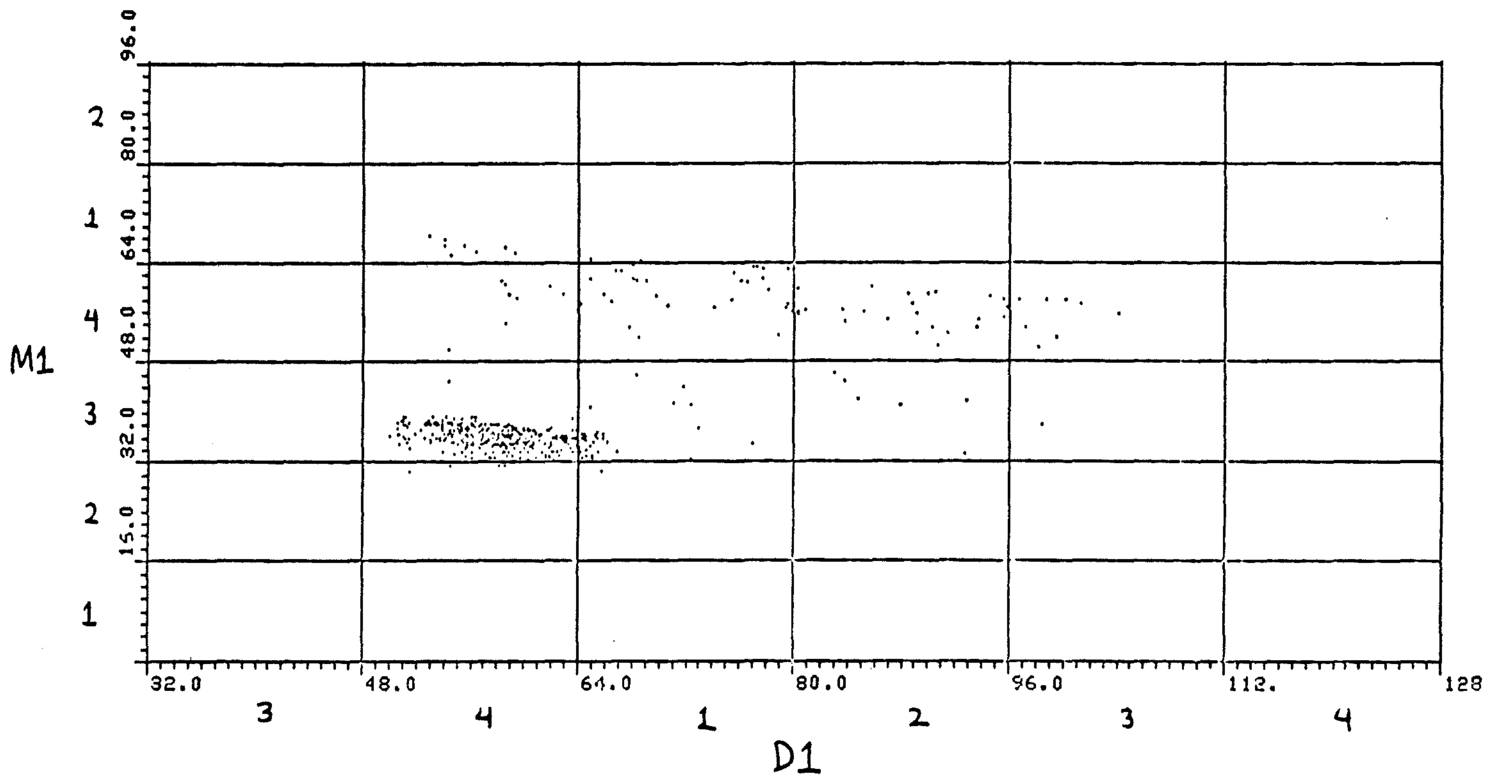

Figure 14. D1 vs. M1 (PHA1 vs. PHA3) plot of range 1 low-Z data from the time period 1978:226-265.

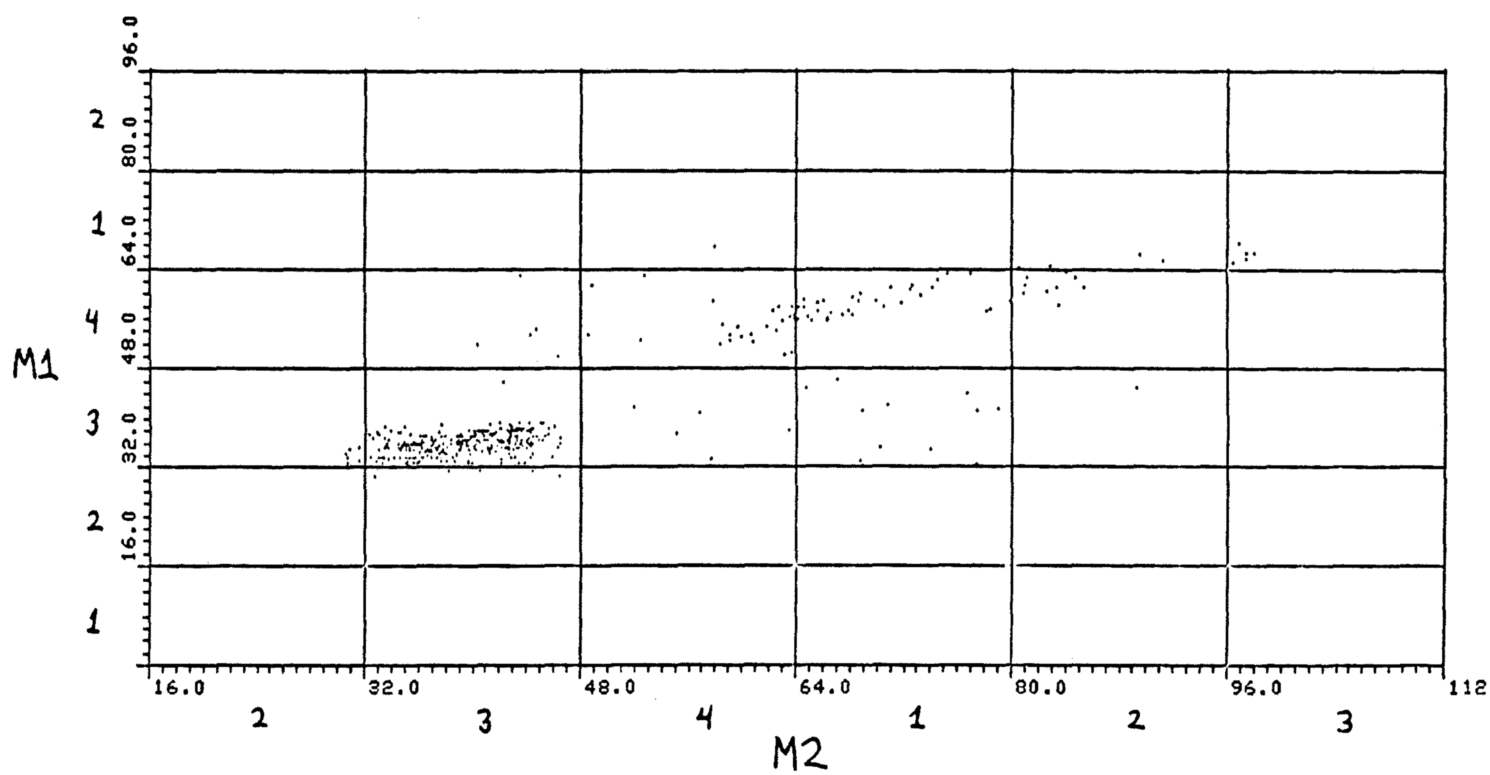

Figure 15. M2 vs. M1 (PHA2 vs. PHA3) plot of range 1 low-Z data from the time period 1978:226-265. Lower track consists of normal protons only.

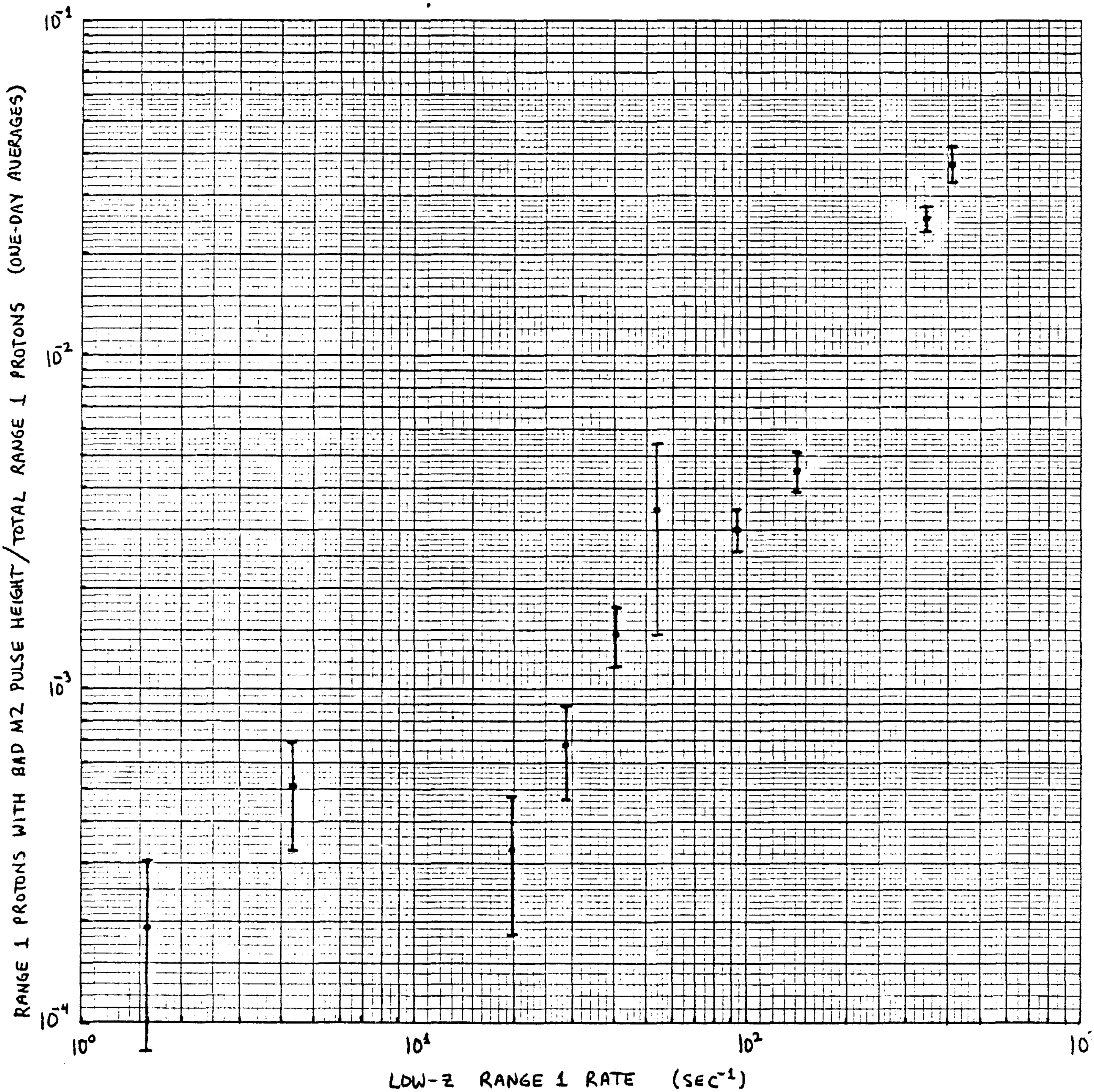

Figure 16. Number of range 1 protons with bad M2 pulse heights, as a fraction of the total number of range 1 protons, vs. low-Z range 1 rate. Each point plotted represents a one-day average.

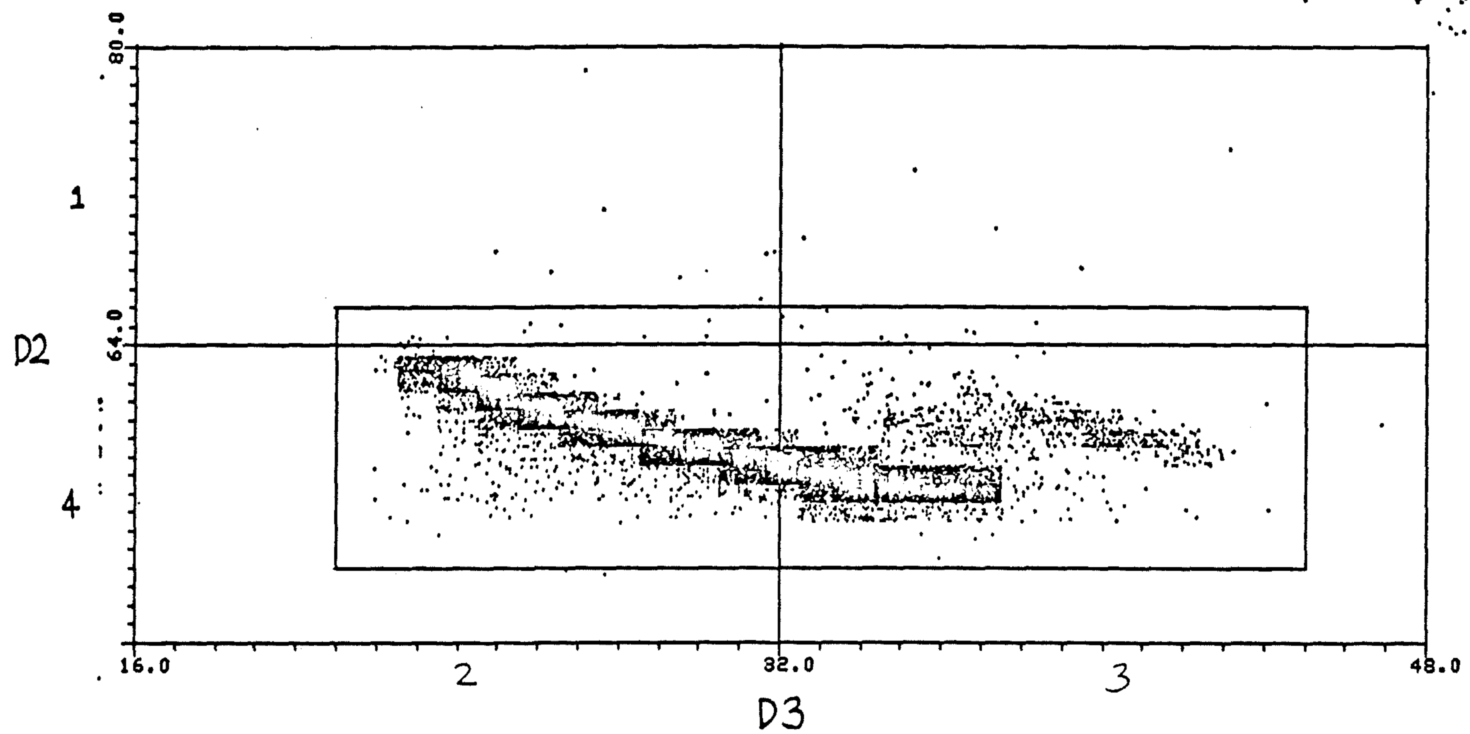

Figure 17. D3 vs. D2 (PHA1 vs. PHA2) plot of range 3 proton data from the time period 1978:267-271. Note spurious proton events near main track.

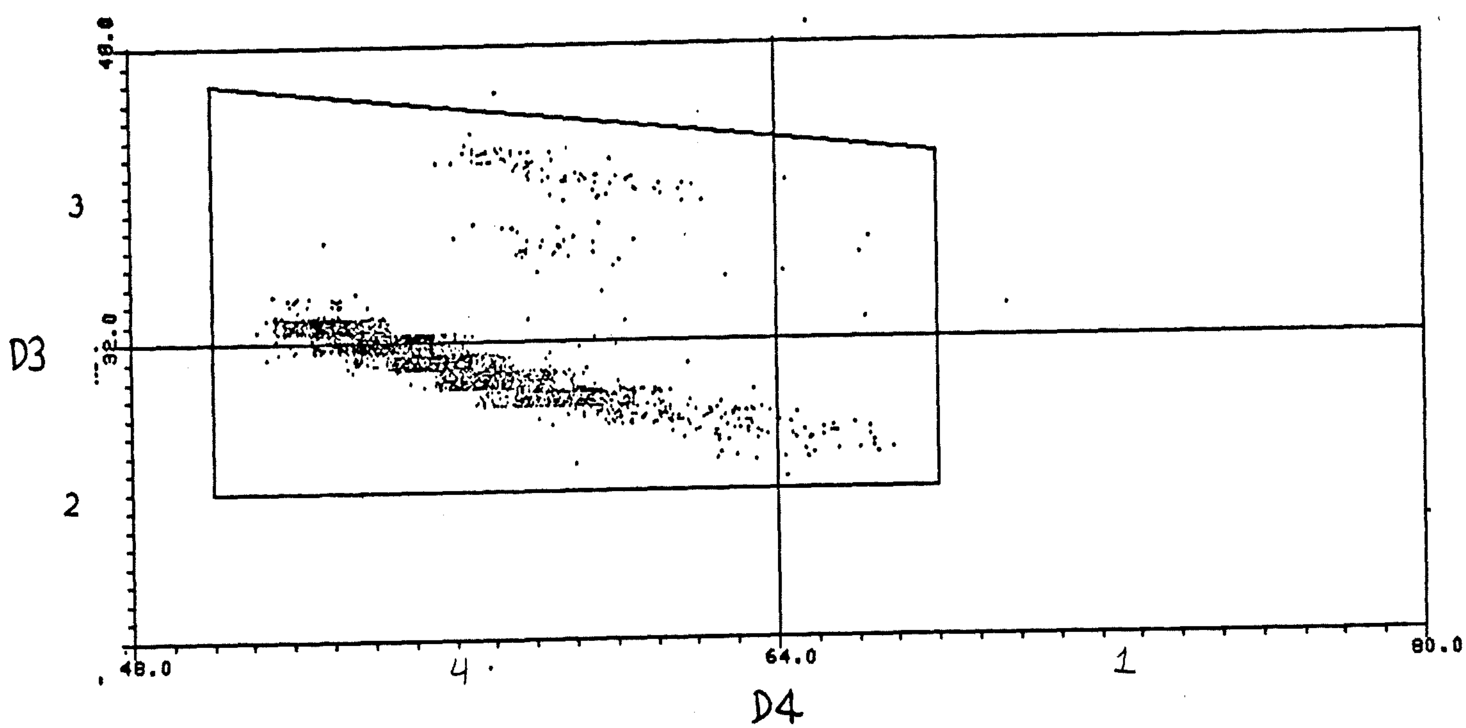

Figure 18. D4 vs. D3 (PHA1 vs. PHA2) plot of range 4 proton data from the time period 1978:267-271. Note spurious proton events near main track.

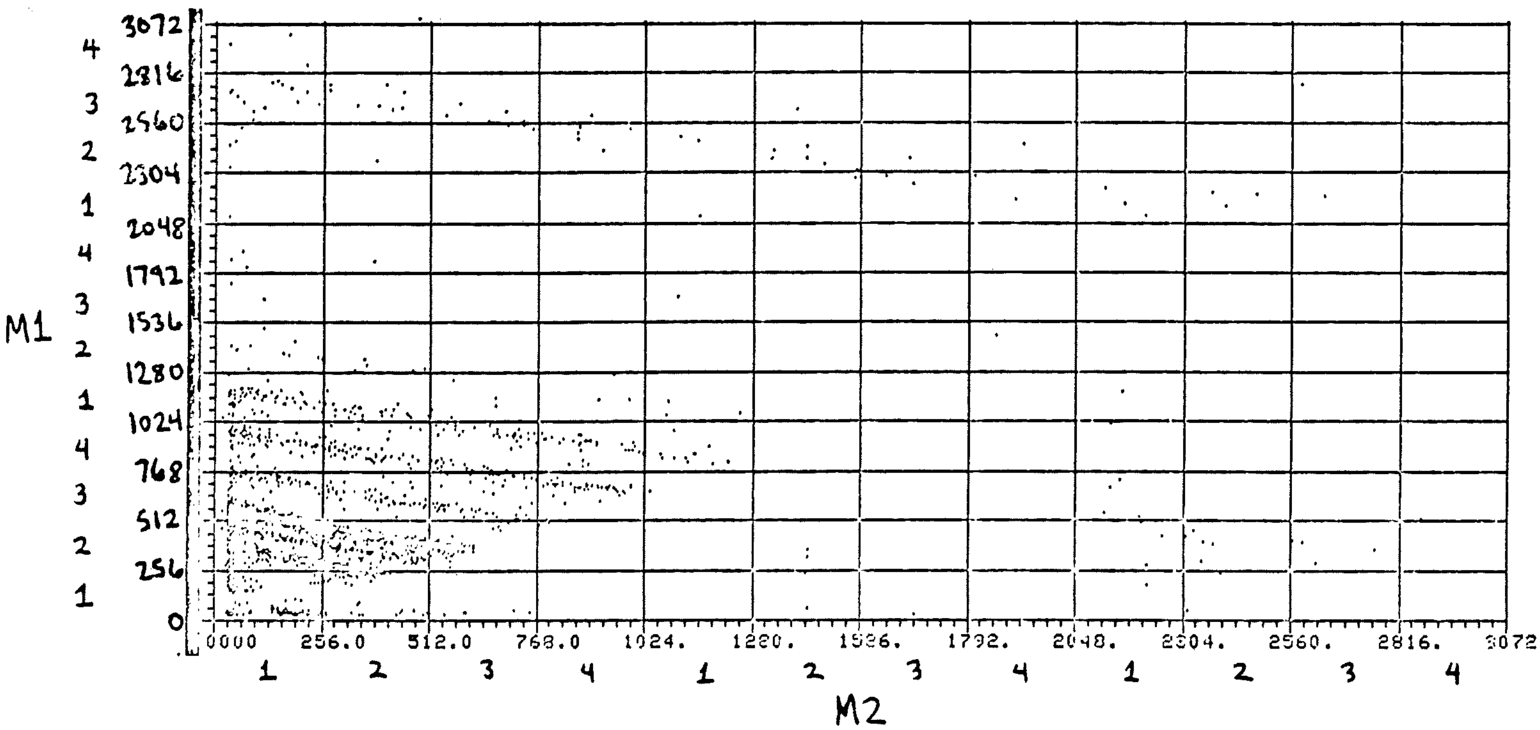

Figure 19. M2 vs. M1 (PHA1 vs. PHA2) plot of range 0 high-Z data from the time period 1978:226-334. Note "bin" digits denoting values of the 256- and 512-channel pulse height bits.

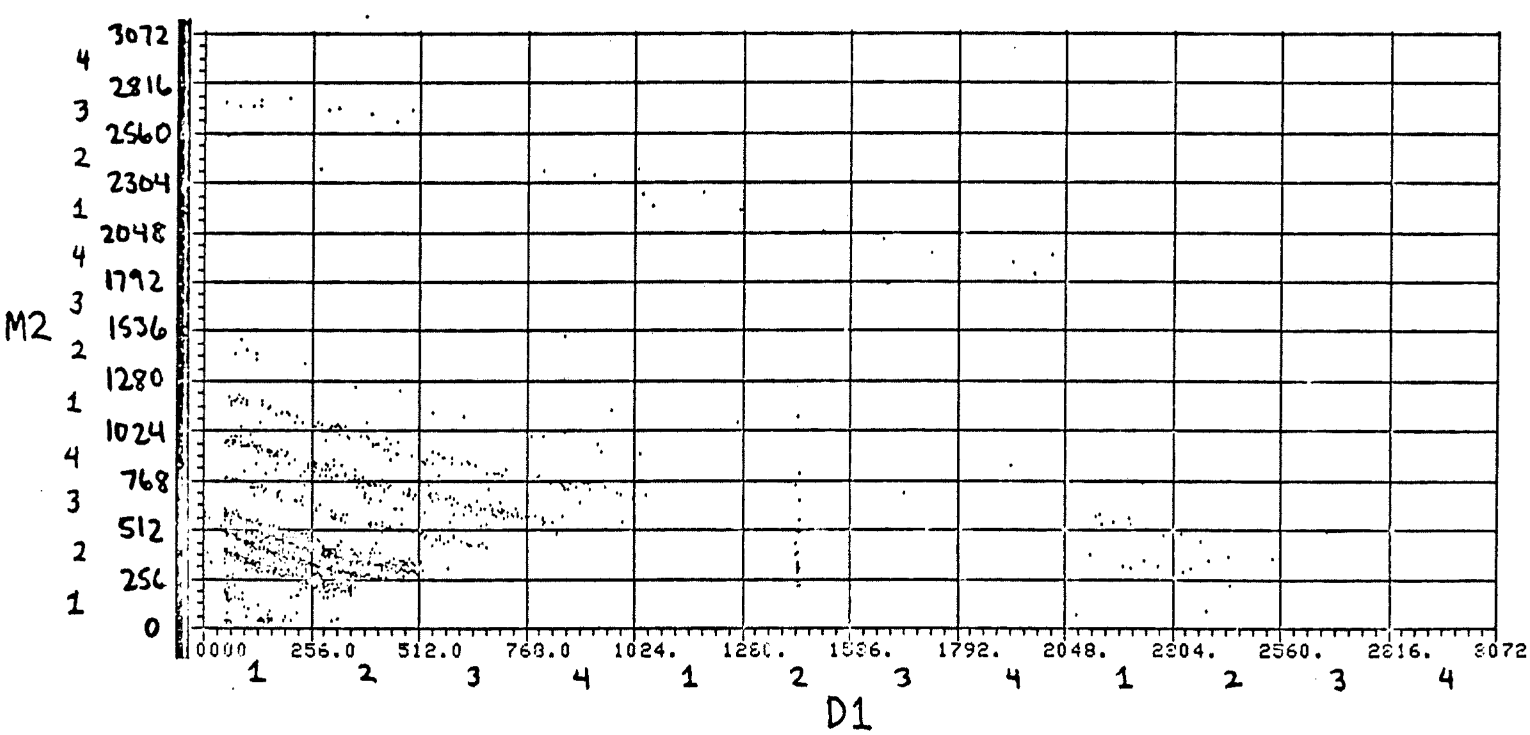

Figure 20. D1 vs. M2 (PHA1 vs.PHA2) plot of range 1 high-Z data from the time period 1978:226-334.

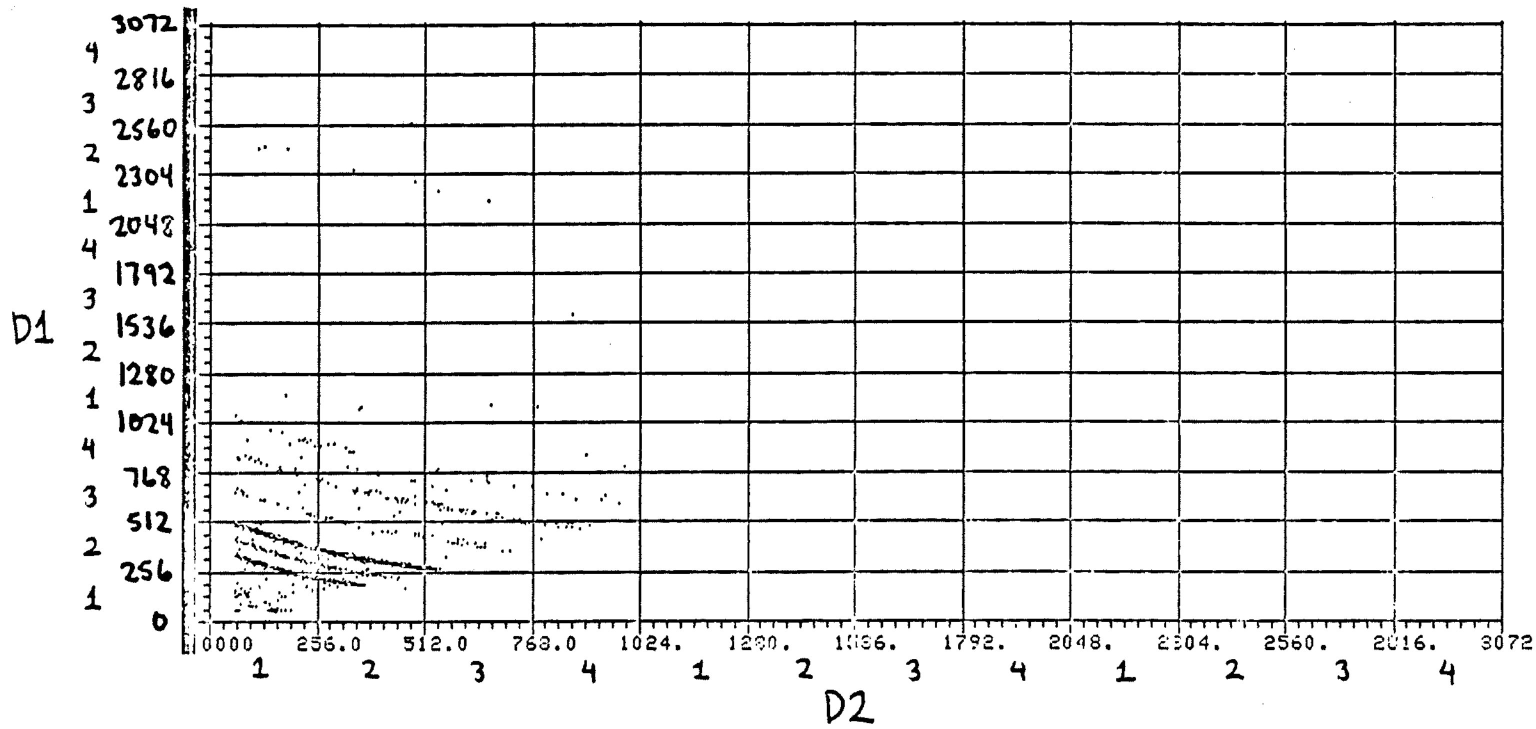

Figure 21. D2 vs. D1 (PHA1 vs. PHA2) plot of range 2 high-Z data from the time period 1978:226-334.

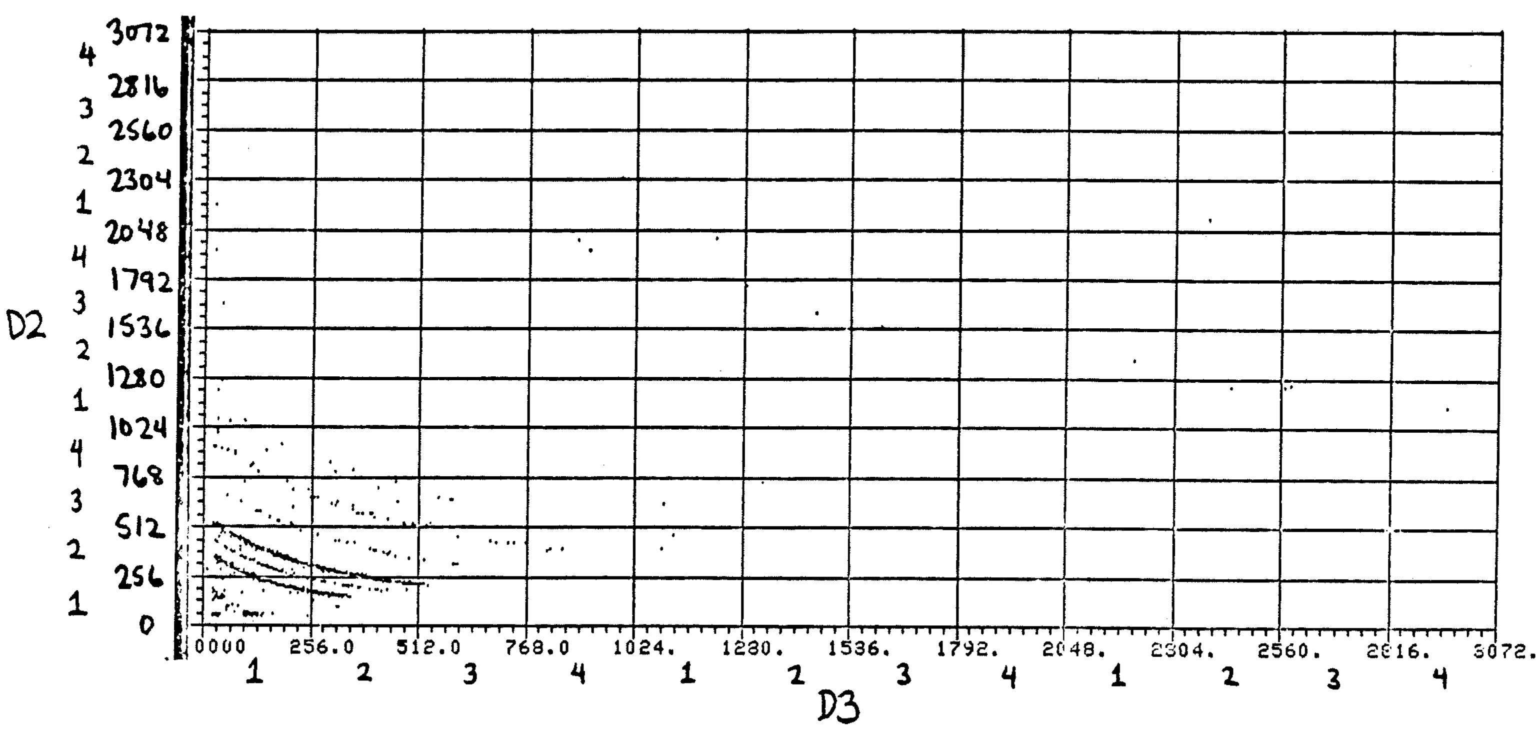

Figure 22. D3 vs. D2 (PHA1 vs. PHA2) plot of range 3 high-Z data from th- time period 1978:226-334.

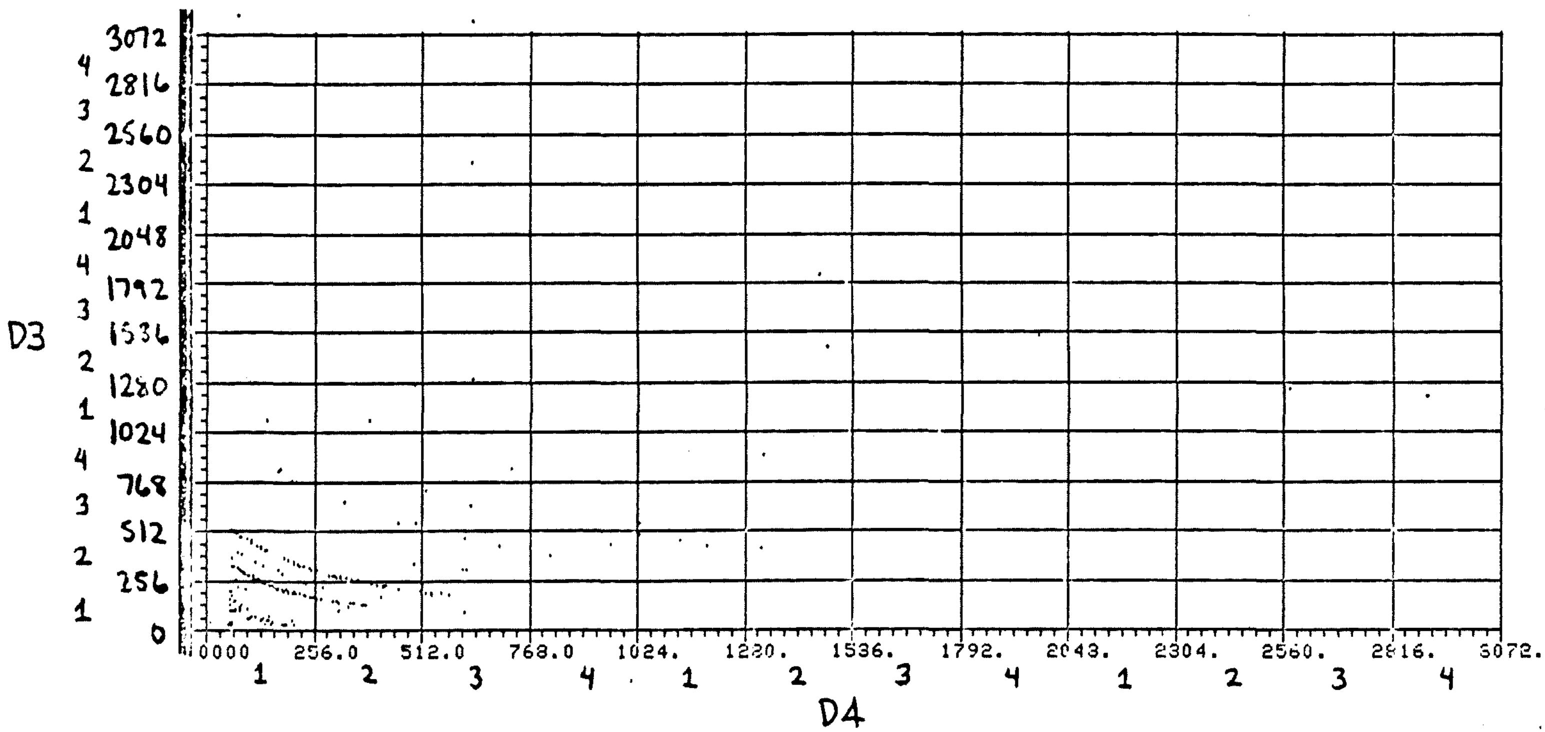

Figure 23. D4 vs. D3 (PHA1 vs. PHA2) plot of range 4 high-Z data from the time period 1978 226-334.

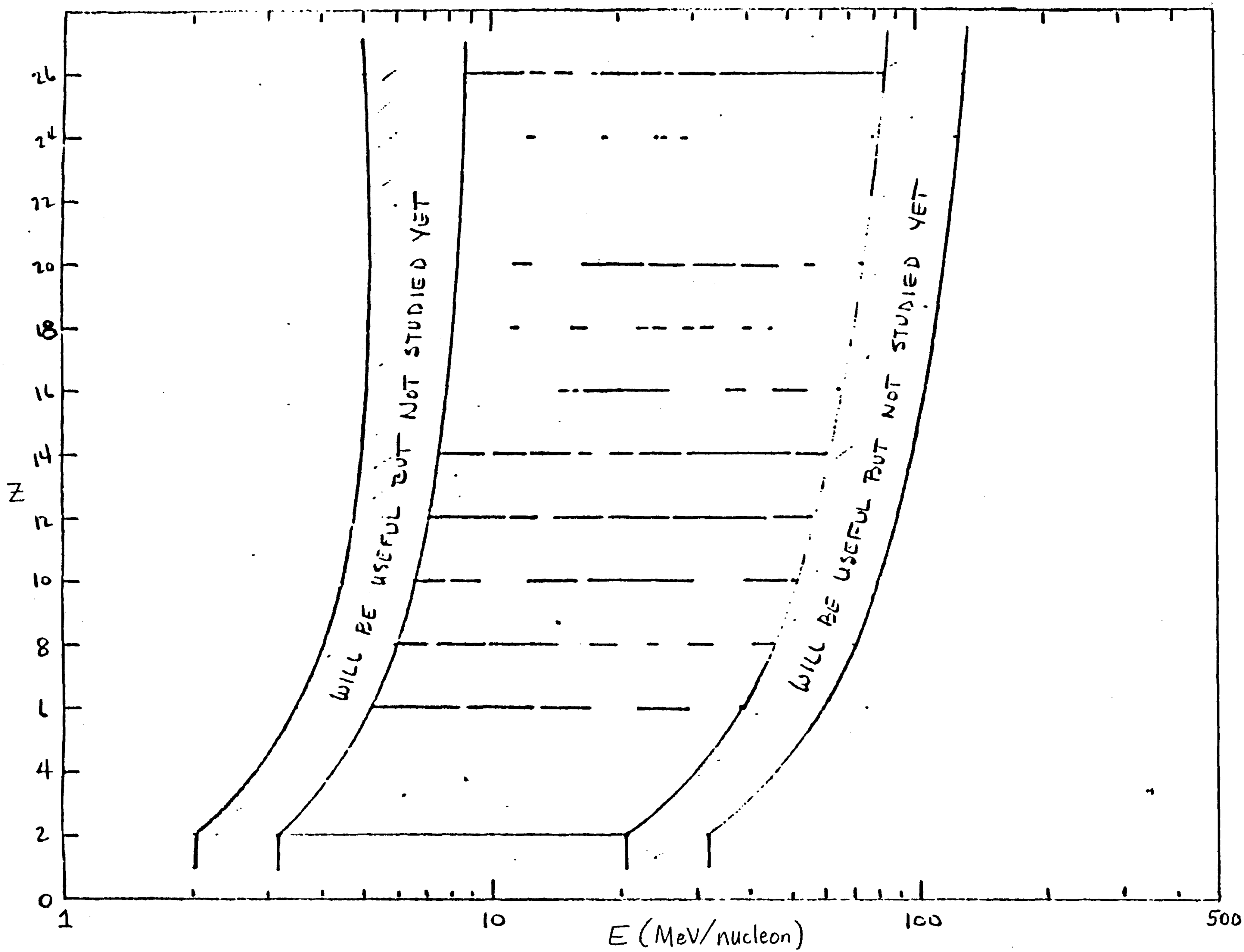

Figure 24. Energy intervals in which even-high-Z elements can be resolved to a purity of at least 80 %.

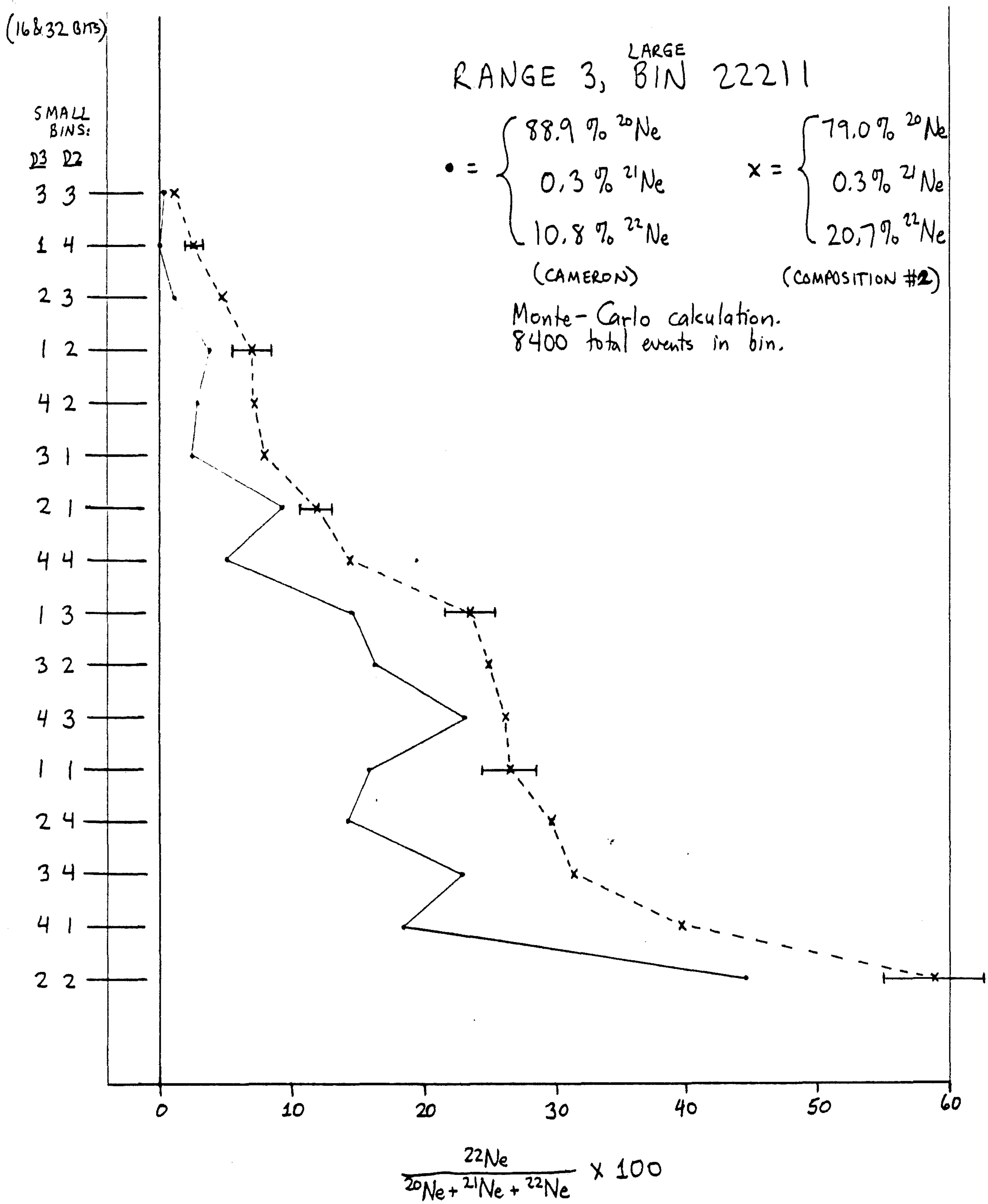

Figure 25. Isotopic composition of 16 "small bins" contained in range 3 "large bin" 22211, for two different overall Ne isotopic composition schemes.